Whitmarsh, R.B., Sawyer, D.S., Klaus, A., and Masson, D.G. (Eds.), 1996
Proceedings of the Ocean Drilling Program, Scientific Results, Vol. 149

26. PETROLOGY OF THE MAFIC ROCKS CORED IN THE IBERIA ABYSSAL PLAIN[1]

Guy Cornen,[2] Marie-Odile Beslier,[3] Jacques Girardeau[2]

ABSTRACT

During Ocean Drilling Program (ODP) Leg 149 to the Iberia Abyssal Plain, drilling into the basement recovered mafic rocks near and east of a north-south peridotite ridge that bounds the Iberian ocean/continent transition. Recovered primarily at Sites 899 and 900, 60 km apart, some of these extrusive and intrusive mafic rocks show evidence of low to high metamorphic grade. Those recovered at Site 899 consist of lavas, microgabbros, and metamorphosed rocks that occur with predominantly ultramafic breccia and sedimentary rocks within a mass-flow deposit. The entire basement core from Site 900 consists of brecciated flaser gabbros.

The low-grade metamorphosed or unmetamorphosed lavas and microgabbros at Site 899 derive from the crystallization of E-MORB to alkaline magmas. Some of the mafic rocks, and particularly the chlorite-bearing schists, may be considered as formerly differentiated Fe-Ti leucogabbros or plagiogranites, later hydrothermally modified under low-temperature and low-pressure conditions. The flaser gabbros (Site 900) and the sheared amphibolites (Site 899) have tholeiitic to transitional affinities, slightly different from those of typical mid-ocean ridge gabbros. These former gabbros underwent intense shearing under relatively high-temperature (high amphibolite to granulite facies) and high-pressure (≥0.8 Gpa) conditions that ended around 136 m.y. ago in lower-grade metamorphic conditions (Féraud et al., this volume).

The peculiar mineralogy, chemistry, and tectonometamorphic evolution of these mafic rocks combined with the preliminary isotope ages are consistent with an origin during continental rifting. The flaser gabbros would have crystallized from transitional to tholeiitic magmas, which ponded and slowly cooled at the base of continental crust, and then sheared during continental extension. Similar, but weakly alkaline, magmas poured out onto the suboceanic floor as extension proceeded. The older ones were subsequently hydrothermally modified under low pressure.

INTRODUCTION

The nature of the basement of nonvolcanic passive continental margins is poorly documented. Their structure and lithology have, however, a critical importance in constraining the beginning of the rifting process. Recent studies of ocean/continent transitions have shown that serpentinized peridotites occur frequently on these nonvolcanic margins. The presence of such mantle fragments at ocean/continent transitions proves that continental break-up does not necessary imply subsequent and immediate oceanic accretion, (i.e., extrusion of a large volume of lavas producing new crust). This was well illustrated on the west Galicia Margin where successive dredges (Boillot et al., 1980), drill holes (ODP Leg 103; Boillot, Winterer, Meyer, et al., 1988; Boillot et al., 1988a, b), and dives using the French submersible *Nautile* (Galinaute cruise; Boillot et al., 1988a) have emphasized that the ocean/continent transition was bordered by a peridotite ridge.

Geophysical survey data (Beslier et al., 1993; Whitmarsh et al., 1990, 1993) and drilling data from Sites 897 and 899, acquired during Leg 149 in the Iberia Abyssal Plain, suggest that this ultramafic ridge extends more than 300 km south of the Galicia Margin (Fig. 1). West of this ridge, an abnormally thin crust with, in places, a seafloor-spreading magnetic signature, remains unsampled. Mafic rocks were recovered in minor amounts near the peridotite ridge itself (Sites 897 and 899), but mainly on a basement high at Site 900, farther east toward the continent. These rocks are irregularly distributed and varied; they are mostly gabbros with minor basalts and dolerites.

On the Galicia Margin, very few mafic rocks were sampled together with the peridotites. They were recovered from five dive sites on the northwestern edge of the bank and consist of a few dioritic veinlets that crosscut the peridotites, 10-m-thick chlorite-bearing schists, supposedly derived from a Fe-Ti-rich gabbro (Beslier et al., 1990; Schärer et al., 1995), a single pod of gabbro, and eight occurrences of basalts and dolerites (Boillot et al., 1988a; Beslier et al., 1990). The chemical signatures and ages of the mafic rocks support a formation during the continental rifting phase (Féraud et al., 1988; Kornprobst et al., 1988; Schärer et al., 1995).

In the Iberia Abyssal Plain, the close association of mafic and ultramafic rocks strongly suggests that magmas were also generated during the rifting stage. To test this hypothesis, petrological data, including phase analyses along with bulk-rock, trace-element, and rare-earth-element chemistry, are discussed and compared to similar occurrences.

SITE CHARACTERISTICS

Sites 897, 899, and 900 were drilled on basement highs within the ocean/continent transition (Fig. 1). Among the several holes drilled at each site, Holes 897C, 897D, 899B, and 900A yielded basement samples.

At Holes 897C and 897D, 100 m apart, the basement was reached under 650 and 680 m, respectively, of Pleistocene to mid-Eocene sedimentary rocks. The basement section recovered is almost completely ultramafic. In Hole 897C, additional rare and small pieces of volcanic breccias were recovered between the ultramafic cobbles of the top of

[1] Whitmarsh, R.B., Sawyer, D.S., Klaus, A., and Masson, D.G. (Eds.), 1996. *Proc. ODP, Sci. Results,* 149: College Station, TX (Ocean Drilling Program).
[2]Laboratoire de Petrologic Structurale, 2 rue de la Houssinière, 44072 Nantes cedex 03, France. Cornen: cornen@chimie.univ-nantes.fr.
[3]Laboratoire de Géodynamique sous-marine, Université Paris 6, BP48, 06230 Villefranche sur Mer, France.

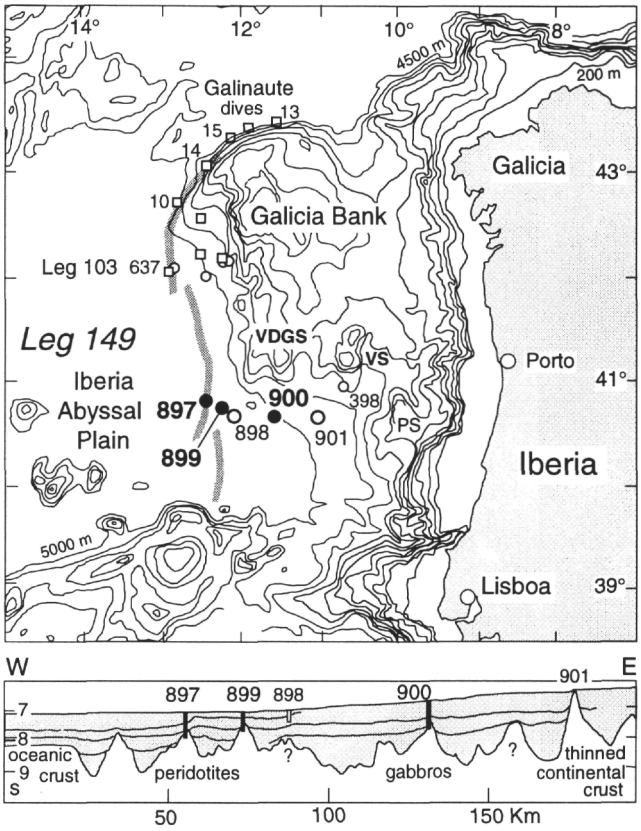

Figure 1. Bathymetric map of West Iberia and cross section through the Iberia Abyssal Plain showing the location of holes drilled during Leg 149. Sites of former drilling (Leg 103) and diving (Galinaute cruise) (open squares) on the Galicia Margin and vicinity are also indicated. The inferred peridotite ridge at the ocean/continent transition is shaded.

the basement section. In Hole 897D, a few pieces of strongly altered basaltic lavas, doleritic rocks, and undeformed microgabbros were recovered from the sediments immediately overlying the basement (Shipboard Scientific Party, 1994a).

About 20 km east-southeast of Site 897, Hole 899B was drilled on a basement high detected during the cruise, at a water depth of 5291 m. At that site, the acoustic basement was reached under 369.9 m of Pleistocene to upper Eocene sedimentary rocks, and over 180 m of basement was cored. The sedimentary column has been divided into three units. Unit IV is basement and was subdivided into Subunits IVA and IVB. Subunit IVA is 95 m thick and is composed of unsorted ultramafic breccias with accessory mafic metamorphosed clasts (Fig. 2). Subunit IVB is a 19-m-thick transition zone consisting of composite serpentinite breccias, basaltic lavas, and sediments underlain by about 78 m of unbrecciated boulders of peridotite with intercalations of siltstone, basaltic lavas, undeformed microgabbros, and mafic metamorphic rocks. The succession of sedimentary layers inserted in Unit IV, down to 540 mbsf, is normal and consists entirely of lower Aptian rocks (Comas et al., this volume). A cataclastic breccia and varied boulders in a mass-flow deposit would be consistent with this puzzling sequence (Shipboard Scientific Party, 1994b).

Hole 900A was drilled at about 60 km east of Hole 899B, at a water depth of 5037 m. At Site 900, the basement was reached under 748.9 m of Pleistocene to Paleocene sedimentary rocks. Over 56.1 m of basement was drilled and 27.71 m of basement core was recovered, composed entirely of sheared gabbros (Shipboard Scientific Party, 1994c).

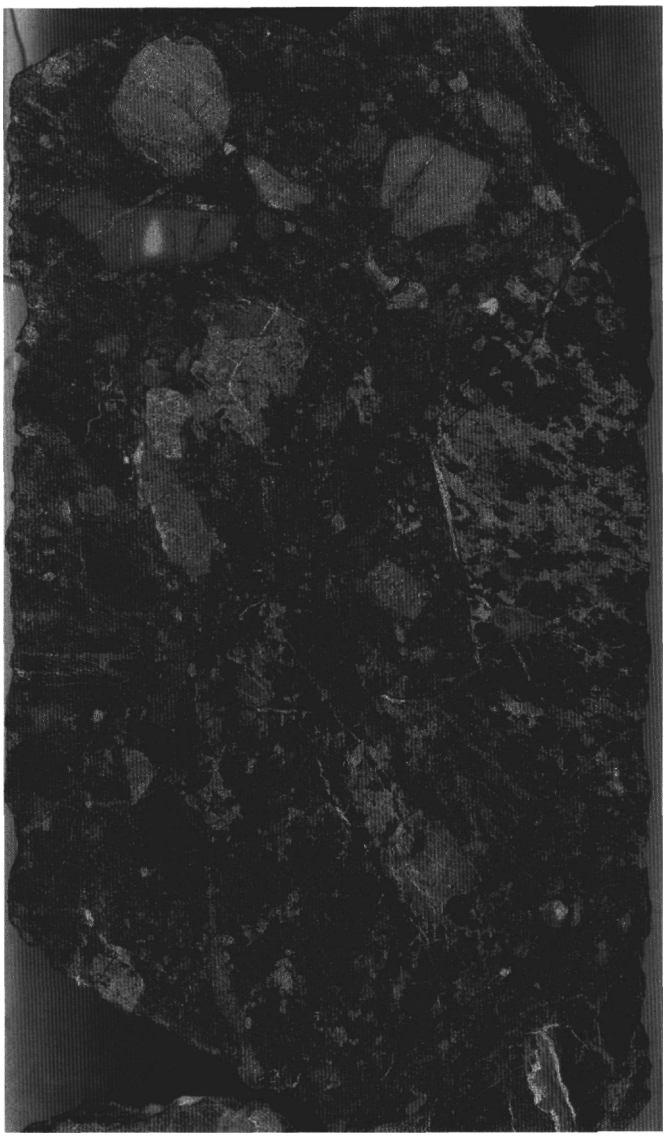

Figure 2. Representative photograph of the ultramafic breccia that comprises Hole 899B, Subunit IVA (Sample 149-899B-20R-3, 80.5-90.5 cm). This sample shows ultramafic clasts (banded gray and black) mixed with fine-grained metamorphosed mafic clasts (light gray) within a serpentinite matrix.

LITHOLOGIC AND PETROGRAPHIC DATA

Unmetamorphosed Lavas and Microgabbros

Unmetamorphosed lavas and micrograbbos were recovered in the lower part of the "basement" section at Site 899, in Subunit IVB. They were found in several intervals, separated by peridotites and lower Aptian sedimentary rocks.

The lavas display either porphyritic, intergranular, or variolitic textures, the latter implying an emplacement on the seafloor. Most of these rocks are deeply altered, as are the finest-grained variolitic lavas, which no longer bear traces of their primary mineralogy. Basalts with intergranular textures generally contain a few relics which allowed microprobe analysis to be done. The basalts contain feldspars, mainly plagioclase, as well as clinopyroxenes, oxides, and accessory minerals, including brown amphibole and biotite, which are restricted to the groundmass. Olivine is rare. When present as a phenocryst, as in variolitic lavas (Sample 149-899B-27R-1, 15-18 cm) (Fig. 3)

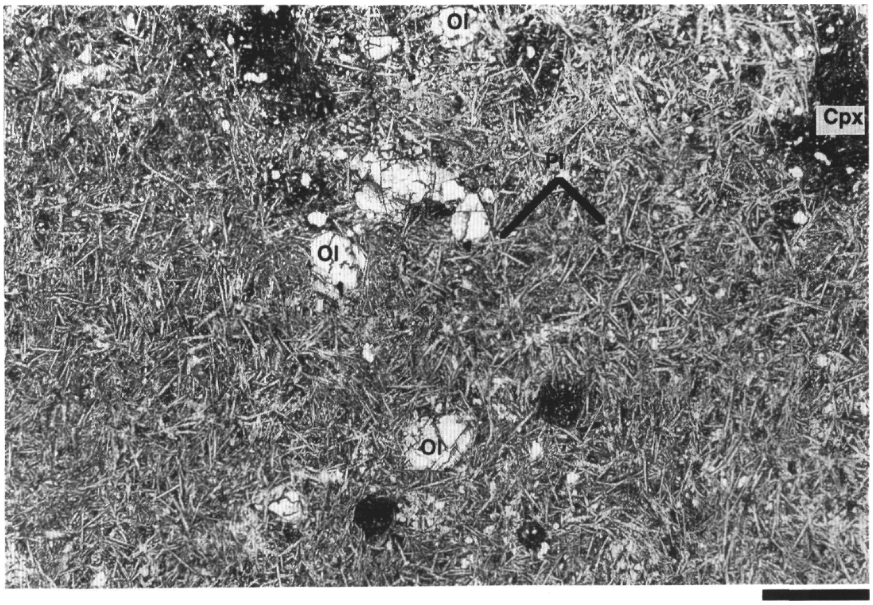

Figure 3. Photomicrograph of a variolitic lava from Hole 899B (Sample 149-899B-27R-1, 15-18 cm; plane-polarized light) in which the primary mineralogy is almost totally transformed. Former olivine phenocrysts (Ol) are recognizable inside a matrix composed mostly of former feathery plagioclase (Pl). Note that some vesicles are filled by quench pyroxenes (Cpx). The bulk-rock analysis of this sample is reported in Table 8. Scale bar is 0.2 mm.

and in porphyritic basalt (Sample 149-899B-27R-1, 27-30 cm), olivine is always replaced by serpentine and smectites. Orthopyroxene was not detected.

The microgabbros were recovered mostly under the basaltic lavas. They have equant textures and a primary mineralogy dominated by plagioclase, clinopyroxene, oxides, and accessory light-brown amphibole and biotite (Fig. 4). All these rocks are strongly altered and contain large amounts of smectite. Rare clasts of similar microgabbros were also found within the ultramafic breccia of Subunit IVA.

Metamorphosed Mafic Rocks

Four types of metamorphosed mafic rock were recovered. They comprise undeformed low-grade metamorphosed basalts and microgabbros, chlorite schists, amphibolites (Site 899), and flaser gabbros (Site 900).

Lavas and microgabbros occur as accessory clasts in the unsorted ultramafic breccia that comprises Subunit IVA in Hole 899B. They are identified by their former intergranular or porphyritic texture, although this is obscured by pervasive prehnite and chlorite. Pyroxenes and oxide remnants may be extant (Fig. 5).

Other fine-grained mafic rocks occur as clasts with equant texture (Subunit IVA) or as boulders with a schistose ones (Subunit IVB). They are composed of at least 90% chlorite. Titanite and/or hydrogarnet, rutile, apatite, and zircon are accessory minerals.

Amphibolites were found as boulders at the bottom of Subunit IVB at Site 899, under the unmetamorphosed lavas and microgabbros. Rare amphibole-bearing clasts invaded by prehnite, included in Subunit IVA, seem to be derived from similar rocks. These amphibolites have a sheared texture and a mineralogy that consists of green and brown amphibole, green spinel, plagioclase, and chlorite. Amphiboles obviously replace porphyroclasts and neoblasts of former pyroxenes. The whole is strongly evocative of amphibolitized flaser gabbros.

The entire basement section recovered at Site 900 is strongly brecciated. Besides this brecciation, the rocks have a dominant greenish white color at the top of the section that grades into grayish green and brown downcore. A clear planar banding is defined by successive mafic and felsic layers. Layers are millimeters thick in the fine-grained intervals, which are dominant, and centimeters thick in the few coarse-grained sections (Figs. 6, 7).

The coarse-grained rocks display typical porphyroclastic textures (Fig. 8) that grade toward granuloblastic ones in the fine-grained sections. In both facies, the "primary" mineralogy is generally preserved and composed of clinopyroxene (up to 60% in fine-grained sections, and about 40% in coarse-grained ones), plagioclase, and rare oxides. Shorebased studies have not detected any orthopyroxene or olivine crystals. Secondary amphibole and chlorite crystals are widespread in the samples. These rocks are typical flaser gabbros.

MINERALOGY AND PHASE CHEMISTRY

Phase compositions have been obtained through a CAMEBAX (SX50) microprobe (Microsonde Ouest, Brest), using silicate and vanadate standards (albite, wollastonite, orthoclase, vanadinite) for calibration of Na, Si, Ca, K, Cl, and oxide standards for calibration of Fe, Mn, Ti, Cr, Al, and Ni. The accelerating voltage was 15 kV, the beam current was 15 nA, and the counting time was between 6 and 25 s, depending upon the analyzed elements. All phases have been analyzed at several places on their cores and margins. Selected data are listed in Tables 1-7.

Pyroxenes

Unmetamorphosed Lavas and Microgabbros

Pyroxenes from lavas with intergranular texture (Site 899) are diopside, with compositions ranging from $Wo_{49}En_{43}Fs_{8}$ to $Wo_{45}En_{43}Fs_{12}$ (Table 1, Fig. 9). They all clearly show an increase in Fe from core to margin of the crystal and a high Ca content. This zonation, together with the obvious correlation that exists between Ti and Al^{IV} (Fig. 10), supports a transitional to alkaline nature for the parent magma (Larsen, 1976). Pyroxenes in the microgabbros from the same site have similar compositions.

In the porphyritic lavas (such as Sample 149-899B-27R-1, 27-30 cm), pyroxenes are restricted to the groundmass and show a quenched habit. They are also diopside, with compositions between $Wo_{47.5}En_{40.3}Fs_{12.2}$ and $Wo_{46.3}En_{31.3}Fs_{22.4}$. These pyroxenes locally indicate a great Fe increase, whereas Al^{IV} and Ti contents remain relatively low.

Metamorphosed Mafic Rocks

Pyroxene remnants were analyzed in mafic clasts which seem to have a former intergranular texture (Samples 149-899B-20R-1, 131-134 cm, 23R-3, 117-120 cm, 27R-2, 7-11 cm), although weakly

Figure 4. Photomicrograph of an undeformed microgabbro boulder from Hole 899B. (Sample 149-899B-35R-1, 29-33 cm). Feldspar (Pl) is almost completely altered. A few remnants of clinopyroxene (Cpx) are indicated (crossed polars). Scale bar = 1 mm.

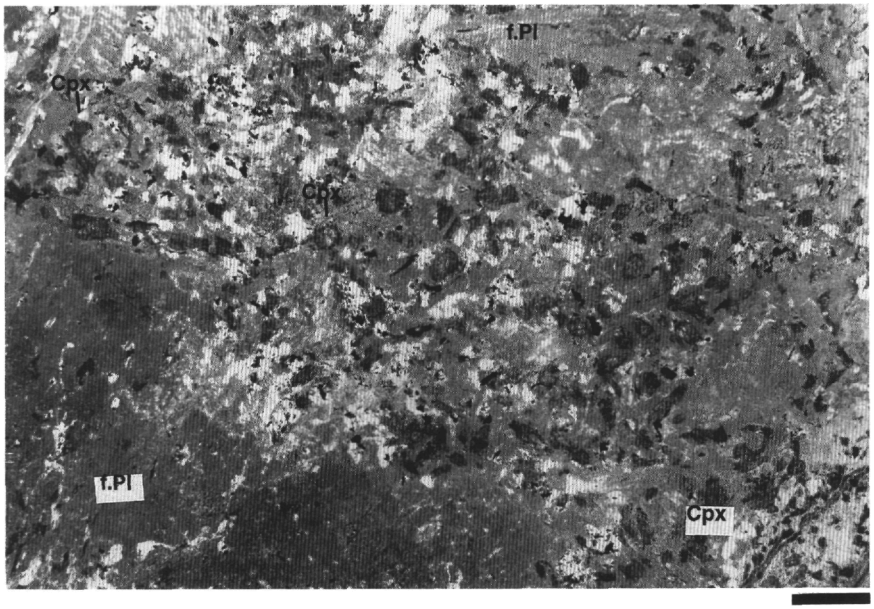

Figure 5. Photomicrogaph of a presumed porphyritic microgabbro (Hole 899B, Subunit IVA, Sample 149-899B-28R-1, 42-45 cm) modified by low-grade metamorphism. Prehnite replaces plagioclase (f.Pl) that initially locally formed phenocrysts and microcrystals. Some relics of pyroxenes (Cpx) and ilmenite (opaques) are still recognizable. Scale bar = 0.1 mm.

metamorphosed and invaded by prehnite. They commonly display a faint and irregular pinkish brown color in plane-polarized light and are locally partly resorbed. In the quadrilateral component diagram (Fig. 9), they show the typical trend of clinopyroxenes from alkaline lavas: Ca content increasing with Fe content. Their Ti contents are lower than those in the unmetamorphosed lavas but are still correlated with Al^{IV}. This correlation includes the pyroxenes from the microgabbro (Fig. 10). It suggests that this low Ti/Al^{IV} trend has not been modified and results from a lower cooling rate (Gamble and Taylor, 1980) rather than from a reequilibration during low-pressure and low-temperature metamorphism. No reliable analyses of pyroxenes are available from metabasalt clasts with apparent porphyritic textures.

In the sheared amphibolites from Site 899, a dominant colorless to slightly green amphibole entirely replaces former pyroxene.

Flaser gabbros from Site 900 commonly exhibit pyroxenes that occur either as porphyroclasts and neoblasts in the porphyroclastic rocks or only as small crystals in the granuloblastic ones. Pyroxene crystals are rarely clear and without defect. They generally display undulose extinctions and, locally, rare exsolution lamellae.

No significant difference has been noticed between the pyroxene porphyroclasts and the neoblasts. They are all diopsides ($Wo_{48.8}En_{42.9}Fs_{8.3}$ to $Wo_{42.7}En_{44.6}Fs_{12.7}$) that display a discrete evolution toward augite ($Wo_{35.1}En_{48.6}Fs_{16.3}$) (Fig. 9). These clinopyroxenes (Table 1) are characterized by high contents of CaO, Al_2O_3, and Na_2O. The high Al content of pyroxenes and their high wollastonite components (or $CaAl_2SiO_6$ molecule) implies crystallization under low silica activity, which is unusual for tholeiitic magmas solidifying under low pressure, such as those recovered from mature slow-spreading ridges including the Mid-Atlantic Ridge (Helmstaedt and Allen, 1977; Honnorez et al., 1984), the Mid-Cayman Rise (Ito and Anderson, 1983), and the Southwest Indian Ridge (Bloomer et al.,1989; Von Herzen et al., 1991).

The Al^{IV}/Al^{VI} diagram (Fig. 11) used to discriminate clinopyroxenes with high- and low-pressure origins (Aoki and Shiba, 1973) clearly shows the difference between the two settings. It emphasizes the compositional similarities of clinopyroxenes from flaser gabbros of Site 900 with those from the metagabbros sampled on Zabargad Island in the Red Sea (Bonatti and Seyler, 1987; Boudier et al., 1988). The range of Al_2O_3 and Na_2O contents of pyroxenes are comparable

Figure 6. Representative photograph of coarse-grained amphibolitized flaser gabbro (Sample 149-900A-82R-5, 13-29 cm). This rock displays a succession of light and dark layers, composed of plagioclase and amphibole replacing pyroxene.

Figure 7. Photograph of a fine-grained flaser gabbro with tight banding (Sample 149-900A-85R-6, 128.5-135.8 cm). Plagioclase layers are dark because their crystals (neoblasts) are rimmed by pervasive chlorite. In contrast, the clinopyroxene layers are bronze- and light-colored. Note their lens shape.

in both places. However, as shown by Figures 11 and 12, metagabbros from Zabargad Island show an obvious decrease in Al from clinopyroxene porphyroclasts to neoblasts that is not detected in rocks from Site 900. Here, porphyroclasts and neoblasts have roughly the same composition, with a slight increase in Al in neoblasts. The absence of orthopyroxene in the Site 900 metagabbros is another difference from those from Zabargad Island.

Feldspar

Unmetamorphosed Lavas and Microgabbros

Two types of feldspar were analyzed in lavas with aphyric and intergranular textures. Feldspars are either phenocrysts with labradorite cores ($Or_{1.4}$ $Ab_{31.6}$ An_{67}) that grade into oligoclase at their periphery, or long laths (200 × 50 µm) and microcrysts of anorthoclase ($Or_{25.1}Ab_{65.9}An_9$ - $Or_{40.5}Ab_{57.5}An_2$) (Fig. 13). These trends are well known in alkaline or in differentiated lavas.

The porphyritic basalts have very different feldspars: phenocrysts and microcrysts grade from $Or_0Ab_{16}Or_{84}$ to $Or_0Ab_{34.7}An_{65.3}$ with some microcrysts around $Or_{3.1}Ab_{66.1}An_{30.8}$. Such a high content of anorthite, unusual in alkaline lavas, fits the composition of feldspar from tholeiitic basalts.

Feldspar in the undeformed microgabbros is generally very altered and partially transformed into clays and, presumably, adularia. Indeed, a potassic feldspar, with a composition close to the potassic end-member, usually rims the plagioclase ghosts. Relics of fresh plagioclase are oligoclase ($Or_{1.4}Ab_{70.9}An_{27.7}$). They are probably of primary origin, although their Or content is low. Such a primary composition would be indicative of slightly differentiated microgabbros.

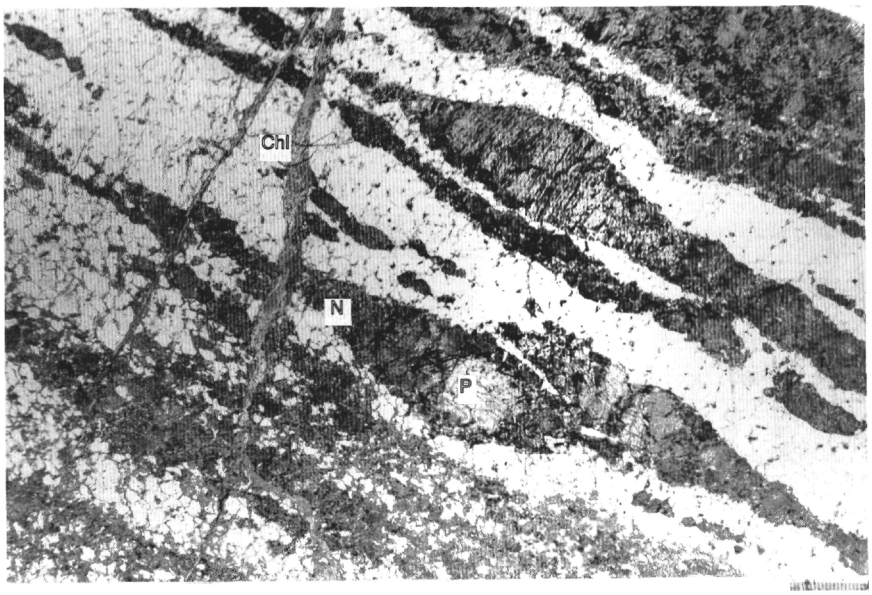

Figure 8. Photomicrograph of a typical flaser gabbro (Sample 149-900A-84R-4, 67-72 cm). The porphyroclastic texture is obvious. The pyroxene porphyroclasts (P) and their neoblast tails (N) delineate the foliation well. Plagioclase neoblasts constitute the light-colored layers and a late chlorite veinlet (Chl) crosscuts the banding. Scale bar = 1 mm.

Metamorphosed Mafic Rocks

In the mafic clast from the Hole 899B (Subunit IVA), prehnite has entirely replaced the feldspar. In the sheared amphibolite from the bottom of this hole, and besides few veins of adularia, feldspar has a restricted range of compositions between $Ab_{35.8}An_{64.2}$ and $Or_{0.2}Ab_{43.6}An_{56.2}$. There is no clear difference in composition between porphyroclasts and neoblasts, although the latter commonly seem slightly richer in Ca (Fig. 14).

Feldspars in the flaser gabbros from Site 900 are either bent porphyroclasts, plastically deformed, or equant neoblasts (Fig. 15). In the fresher rocks, porphyroclasts and neoblasts have similar compositions that range from $Or_{0.3}Ab_{27.6}An_{72}$ to $Or_{0.6}Ab_{45.5}An_{53.9}$ (Table 2). In the highly amphibolitized types, which mostly correspond to the coarser-grained sections of this site, feldspar is generally transformed into albite or even into analcime. However, the presence of Ca-rich plagioclase relics (up to An_{85}) suggests that these amphibolitized sections probably had a composition not strictly comparable to that of clinopyroxene-bearing zones or that they were subjected to different conditions of temperature and water pressure.

Oxides

Unmetamorphosed Lavas and Microgabbros

The porphyritic lavas contain only a titanomagnetite with a high Mn content (7% MnO). Their low sum of oxide components is indicative of alteration (Tables 3, 4). Both titanomagnetite and ilmenite coexist in the aphyric lavas and microgabbros. Unfortunately, they show subsolidus exsolutions and high Mn contents that preclude any thermobarometric estimates relevant to their formation. A high Mn content is noticeable in ilmenite, particularly in the microgabbros, where MnO reaches 2.8 wt%. In comparison, the Fe-Ti gabbros cored in the Indian Ocean contain ilmenites with MnO content between 0.6 and 1.5%-1.7% (Von Herzen et al., 1991). High MnO contents usually characterize oxides from differentiated magmas (Guérin et al., 1979; Frost and Lindsley, 1991).

Metamorphosed Mafic Rocks

Fe-Ti Oxides

In the metabasite clasts from the breccia of Site 899, no magnetite was detected and only ilmenite has been analyzed. It is characterized by high Mn content, which also indicate a common origin for most of the fine-grained metabasite clasts and the microgabbros.

The very low content of magnetic minerals in the rocks from Site 900 correlates well with the low magnetic susceptibility measured on board and the weak magnetic signal recorded over the site (Shipboard Scientific Party, 1994c). Ilmenite is the only Fe-Ti oxide detected. A unique section (Section 149-900A-81R-1) exhibit a high magnetic susceptibility and the presence of Ti and V peaks in bulk-rock analyses. These anomalies correlate with the presence of a higher content of opaques, identified here as altered ilmenite. This phase appears frequently as nuggets within complex associations of titanite and pure Ti-oxides. Again, these ilmenites show high manganese content (Table 4).

Spinel

Green spinels occur in the sheared amphibolites recovered at the bottom of Hole 899B. They are Al- and Fe-rich pleonaste, with Mg# (Mg# = 100 ×Mg/(Mg + Fe + Mn) between 45% and 50% and very low Cr# (<1) (Cr# = Cr × 100/[Cr + Al]) (Table 3).

Flaser gabbros that still contain well-preserved pyroxenes and calcium-rich plagioclase (e.g.. Samples 149-900A-80R-2, 127-132 cm, 84R-4, 67-72 cm, 85R-1, 83-88 cm, 85R-4, 114-120 cm) also contain small green spinel generally located inside the plagioclase neoblasts (Fig. 16). These spinels have low Zn and Ti contents. They are enriched in Al and Fe (Mg# between 35% and 54%), and poor in Cr, (with Fe^{3+} < 4% of the total amount of the trivalent cations), like typical pleonaste. Their presence instead of magnetite explains the low magnetic signature of these flaser gabbros.

The origin of these green spinels in uncertain. Their low Mg# and very low Cr contents are characteristic of metamorphic spinels. Aluminous spinels are common in metabasites metamorphosed in granulite facies conditions (Frost, 1991). Typically, however, green spinels appear in coronitic reactions or as clouds in plagioclase crystals, as observed in coronitic metagabbros from the Adirondack Mountains (Whitney, 1972). Their formation is according to the following reaction:

olivine + plagioclase = orthopyroxene + clinopyroxene + spinel,

which occurs at high pressures (about 0.8 GPa; Frost, 1976). Unfortunately, we found no olivine or orthopyroxene remnants in the flaser gabbros as evidence of this reaction.

Alternatively, we may consider such gabbros to be derived from magmas, the composition of which was not very far from that of the plagioclase- and spinel-bearing websterites recovered at Site 897 (Cornen et al., this volume). Such a possible link remains to be substantiated.

Amphibole and Biotite

Unmetamorphosed Lavas and Microgabbros

Scarce amphiboles, up to 50-200 µm in size, have been found in the mesostasis of doleritic basalts cored at Hole 899B. With more than 0.5 Ti cations per formula unit, these amphiboles are typical kaersutites, which are common in alkaline lavas (Table 5, Fig. 17). The scarce euhedral brown amphiboles found in the undeformed gabbros from the same hole are also rich in Ti and alkalis. They are probably titanian-richterites (Table 5), according to the nomenclature of Leake (1978). This type of amphibole clearly indicates the alkaline affinity of the parental magma.

Both the aphyric lavas and undeformed microgabbros contain some minor biotite, up to 50-100 µm in size, of similar composition. Biotites from the lavas are, however, relatively richer in Fe and Ti (Mg# = 52%, TiO_2 = 7.3%, close to the probable maximum) than those from the undeformed gabbros (Mg# = 55% and TiO_2 = 5%). Their presence in both types of rocks agrees well with the alkaline affinities presumed for their parental magmas. The porphyritic lavas do not contain any of these minerals.

Metamorphosed Mafic Rocks

The sheared amphibolites (Site 899) are mainly composed of plagioclase and of brown and green to colorless amphiboles. These amphiboles are strongly granulated. Brown amphiboles are titanian pargasites with high Cl and low Cr contents (Table 6, Fig. 17). Their high Ti and Al^{IV} contents are indicative of crystallization in amphibolite facies conditions, at higher temperatures than amphiboles from the flaser gabbros of Site 900. Locally, their original chemistry has been modified, probably in association with the intense shearing. The sheared amphibolites display significant decreases in Ti, K, Na, and Cl, and they are retrometamorphosed into magnesiohornblende.

In the flaser gabbros (Hole 900A), amphiboles are clearly secondary phases. Unlike the plagioclase and pyroxenes, they are not granulated. They form either tabular crystals, with cleavages frequently oblique or perpendicular to the foliation, or colorless small fibrous crystals. The tabular crystals commonly exhibit a fibrous appearance and display a faint green color. Their compositions (Table 6, Fig. 17) range from actinolite (low alkali content) to actinolitic hornblende, close to the magnesiohornblende field. They have low Ti, Cr, and Cl contents. These amphiboles are indicative of low-pressure and low-temperature metamorphism within the greenschist grade (Agrinier et al., 1988).

Chlorite, Prehnite, and Epidote

The different types of metamorphosed mafic rocks described in previous sections contain various amounts of secondary phases: mainly secondary amphiboles, chlorite, and prehnite, with subordinate accessory phases such as titanite, hydrogarnet, epidote, opaque minerals, and zeolite.

Among these well-known products of low-grade metamorphism in oceanic rocks (see Agrinier et al., this volume), only the composition of some chlorite-bearing clasts and boulders from Hole 899B will be discussed here. In a clast from Subunit VIA (Sample 149-899B-21R-5, 38-42 cm), as well as in a boulder from the bottom of the hole (Sample 149-899B-37R-1, 27-33 cm), these rocks are almost entirely composed of a bright-blue chlorite (between crossed polars). This "blue" chlorite is a Fe-rich ripidolite that locally is accompanied by titanite, hydrogarnet, apatite, and, more rarely, by zircon and rutile. These ripidolites differ significantly from the clinochlore that locally rims spinels in ultramafic blocks recovered in the same hole; they differ also from those found in sheared amphibolites and flaser gabbros which have a higher Mg# (Table 7).

Because of their mineralogy, it is likely that these chlorite- and titanite-bearing rocks formed under greenschist facies conditions. The common association of inherited and unstable rutile emphasizes the retrograde nature of the metamorphism that likely involved a former Fe- and Ti-rich rock. A sample with a quite similar mineralogy (Schärer et al., 1995) was recovered previously at the top of the peridotite section west of Galicia Bank (Dive 10; Beslier et al., 1990). The chemical meaning will discussed below.

In other mafic clasts, epidote, prehnite, and Al-chlorite crystallized close to equilibrium conditions. According to Liou et al. (1985), such an association, together with the absence of pumpellyite, is indicative of pressure-temperature conditions with a wedge shape (in pressure-temperature space) between 200° and 400°C and a maximum pressure of 0.22 GPa.

GEOCHEMISTRY

Table 8 lists the major elements, main trace elements, and rare-earth elements (REE) that were analyzed in selected rocks, to complement the shipboard analyses. Analyses were conducted on the most representative and the least altered lithological types: lavas, microgabbros, mafic metamorphosed rocks, and flaser gabbros. A few extensively altered samples, for which no primary phases are still extant, were also included.

Unmetamorphosed Lavas and Microgabbros

The undeformed lavas (with aphyric or intergranular textures) and the microgabbros from Site 899 have similar compositions. They have low SiO_2 contents (<46%), MgO content around 10%-12%, and Mg# (= 100 ×Mg/[Mg + Fe]) between 83% and 87%. Two groups of TiO_2 contents are recorded, with values close to 0.6% and 1%, respectively. They separate porphyritic lavas (0.6%) from other lavas, including microgabbros. High loss-on-ignitions (LOIs) imply high degrees of alteration and cast suspicion on the primary origin of the alkalis, especially the high content of K_2O nearly equal to Na_2O (Table 8). This precludes the derivation of firm conclusions from diagrams based on alkali contents and CIPW norms.

The chondrite-normalized REE patterns obtained for the various types of lava and for the microgabbro from Site 899 are contrasted. The variolitic and intergranular lavas, as well as the microgabbro, all display significant light REE (LREE) enrichments (Fig. 18). In the lavas, enrichment reaches 50 times chondrite for La, with a Ce_N/Yb_N ratio of 5.05. In the microgabbro, enrichment reaches 15 times chondrite, with Ce_N/Yb_N = 1.28. This indicates a transitional to alkaline origin for their parental magmas. The microgabbro displays a positive Eu anomaly, associated with plagioclase accumulation, a feature that is absent in the lavas. Though weakly cumulative, this microgabbro has a pattern similar to those from E-MORB. The porphyritic lava displays a rather flat REE pattern, at about 10 times chondrite, without detectable LREE depletion.

Metamorphosed Mafic Rocks

Relatively immobile elements such as Al, Mg, and Ti successfully discriminate the origins of clasts found in the ultramafic breccia at Site 899. The amphibolitized ultramafic clasts have Al_2O_3 < 12% and MgO > 37%, (wt% of anhydrous rock) whereas the metamorphosed mafic ones have Al_2O_3 > 14% and MgO < 18% (Table 8).

The prehnite-bearing mafic clasts are characterized by low SiO_2 contents (34%-39%), by very low alkali, Rb, and Sr contents coupled with high Al_2O_3 and CaO (10%-15%) contents, and by high LOIs (7%-11%). Such a secondary chemical signature was probably acquired during the low-grade metamorphic event. As for the unmetamorphosed lavas and microgabbros, TiO_2 contents discriminate two

Table 1. Selected analyses of pyroxenes.

Hole:	899B			899B		899B			899B		899B				899B	900A
Core, section:	20R-1			27R-1		27R-1			27R-2		28R-2				34R-1	80R-2
Interval (cm:)	134–136			27–30		33–40			7–11		8–10				37–42	95–96
Sample	Metamicrogabbro (clast)			Porphyritic basalt		Doleritic basalt			Metabasalt (clast)		Doleritic basalt				Micro-gabbro	Flaser gabbro
Site:	C	C	M	μ	μ	C	C	M	C	C	C	M	C	M	C	C
Major elements																
SiO_2	49.91	52.52	50.75	48.74	47.44	48.81	48.71	49.09	51.36	51.77	47.60	46.63	48.49	45.70	51.41	51.10
TiO_2	1.28	0.52	0.86	1.39	2.74	2.22	2.23	2.01	0.00	0.09	2.67	3.01	2.57	3.66	1.00	0.77
Al_2O_3	4.47	2.37	2.20	3.93	3.89	4.94	5.05	4.04	3.60	2.33	6.48	5.45	5.29	6.57	3.05	4.76
Cr_2O_3	0.00	0.00	0.00	0.11	0.00	0.22	0.06	0.05	0.03	0.18	0.14	0.00	0.05	0.00	0.12	0.33
FeO	7.31	5.79	10.07	11.05	15.31	8.55	8.82	8.49	7.49	8.24	6.30	11.39	6.97	10.51	6.97	6.01
MnO	0.02	0.04	0.40	0.39	0.33	0.29	0.21	0.26	0.16	0.27	0.15	0.27	0.08	0.32	0.36	0.14
NiO	0.00	0.00	0.00	0.00	0.00	0.00	0.00	0.00	0.00	0.00	0.08	0.01	0.12	0.00	0.03	0.00
MgO	15.19	17.68	13.90	12.92	9.81	13.88	14.02	13.61	15.96	14.29	14.23	11.13	14.12	11.91	15.30	14.92
CaO	20.89	21.09	21.82	21.14	20.19	20.50	20.04	21.62	20.22	22.90	21.90	21.26	21.81	21.27	21.29	21.67
Na_2O	0.73	0.33	0.51	0.45	0.62	0.52	0.51	0.47	0.19	0.25	0.32	0.51	0.34	0.50	0.30	0.69
K_2O	0.00	0.00	0.00	0.00	0.02	0.02	0.00	0.02	0.05	0.00	0.02	0.00	0.00	0.00	0.00	0.00
Total	100.23	100.63	100.99	100.58	100.67	99.94	99.64	99.64	99.08	100.31	99.88	99.66	99.83	100.43	99.93	100.39
Si	1.836	1.907	1.882	1.825	1.813	1.815	1.816	1.834	1.904	1.915	1.761	1.769	1.800	1.712	1.900	1.867
Al^{IV}	0.164	0.093	0.096	0.173	0.175	0.185	0.184	0.166	0.096	0.085	0.239	0.231	0.200	0.288	0.100	0.133
Al^{VI}	0.030	0.009	0.000	0.000	0.000	0.032	0.038	0.011	0.061	0.016	0.043	0.013	0.031	0.002	0.033	0.072
Ti	0.036	0.014	0.024	0.039	0.079	0.062	0.062	0.056	0.000	0.002	0.074	0.086	0.072	0.103	0.028	0.021
Cr	0.000	0.000	0.000	0.003	0.000	0.006	0.002	0.001	0.001	0.005	0.004	0.000	0.001	0.000	0.003	0.009
Fe^{3+}	0.115	0.079	0.128	0.129	0.089	0.061	0.056	0.075	0.051	0.077	0.067	0.084	0.049	0.116	0.029	0.058
Fe^{2+}	0.110	0.097	0.185	0.217	0.401	0.205	0.219	0.190	0.182	0.178	0.128	0.278	0.168	0.214	0.186	0.126
Mn	0.001	0.001	0.012	0.012	0.011	0.009	0.007	0.008	0.005	0.008	0.005	0.009	0.003	0.010	0.011	0.004
Ni	0.000	0.000	0.000	0.000	0.000	0.000	0.000	0.000	0.000	0.000	0.003	0.000	0.005	0.000	0.001	0.000
Mg	0.833	0.957	0.769	0.721	0.559	0.769	0.779	0.758	0.882	0.788	0.784	0.629	0.781	0.665	0.843	0.812
Ca	0.823	0.820	0.867	0.848	0.827	0.817	0.800	0.865	0.803	0.907	0.868	0.864	0.867	0.854	0.843	0.848
Na	0.052	0.023	0.036	0.033	0.046	0.038	0.037	0.034	0.014	0.018	0.023	0.038	0.024	0.036	0.022	0.049
K	0.000	0.000	0.000	0.000	0.001	0.001	0.000	0.001	0.002	0.000	0.001	0.000	0.000	0.000	0.000	0.000
Total	4.000	4.000	4.000	4.000	4.000	4.000	4.000	3.999	4.001	3.999	4.000	4.001	4.001	4.000	3.999	3.999
Wo	46.61	43.78	47.63	47.48	46.28	45.60	44.52	47.72	43.02	48.44	48.75	48.80	47.77	49.29	45.02	47.48
En	47.16	51.06	42.21	40.35	31.29	42.95	43.32	41.79	47.25	42.05	44.07	35.53	43.00	38.39	45.03	45.48
Fs	6.23	5.17	10.16	12.17	22.43	11.46	12.16	10.49	9.74	9.51	7.18	15.68	9.23	12.33	9.95	7.04

Notes: C = phenocryst or porphyroclast core, M = phenocryst or porphyroclast margin, μ = microcryst, N = neoblast. Formula unit calculated on the basis of 6 oxygens and 4 cations. Wo, En, Fs = molecular proportion of wollastonite, enstatite, and ferrosilite.

Table 1 (continued).

Hole:	900A	900A	900A	900A	900A	900A
Core, section:	84R-4	84R-4	85R-1	85R-1	85R-4	85R-5
Interval (cm:)	67–72	131–133	21–24	83–88	114–120	30–32

Sample	Flaser gabbro																
Site:	C	M	C	C	M	N	C	M	N	C	C	M	N	N	C	C	C
Major elements:																	
SiO_2	50.85	50.00	52.52	50.77	50.96	52.23	50.99	51.26	50.07	52.20	49.73	50.25	49.44	51.35	50.84	50.68	50.55
TiO_2	0.81	0.93	0.43	0.77	0.58	0.36	0.65	0.75	0.78	0.70	0.76	0.81	1.07	0.79	0.83	0.67	0.70
Al_2O_3	5.33	6.52	4.20	5.45	6.09	4.35	6.07	5.05	7.04	3.42	7.27	6.21	6.37	4.67	5.16	6.06	6.09
Cr_2O_3	0.19	0.09	0.08	0.21	0.16	0.00	0.21	0.46	0.19	0.08	0.26	0.06	0.18	0.08	0.17	0.23	0.01
FeO	7.50	7.82	6.17	6.14	6.36	7.04	6.51	6.64	7.20	6.99	6.62	6.73	6.91	5.66	6.46	6.90	6.21
MnO	0.24	0.29	0.17	0.13	0.22	0.18	0.24	0.25	0.20	0.14	0.18	0.20	0.14	0.15	0.16	0.14	0.09
NiO																	
MgO	13.66	13.21	15.14	14.07	14.01	15.27	13.73	14.29	13.79	14.38	13.47	13.76	13.74	14.72	14.08	13.59	13.61
CaO	21.17	20.40	21.06	21.42	21.63	20.21	20.88	21.42	20.85	21.63	21.31	21.51	21.62	21.98	21.15	21.10	21.60
Na_2O	0.68	0.79	0.66	0.71	0.67	0.59	0.86	0.72	0.84	0.55	0.87	0.67	0.65	0.57	0.68	0.77	0.74
K_2O	0.00	0.00	0.00	0.00	0.00	0.01	0.00	0.00	0.03	0.01	0.00	0.04	0.00	0.00	0.00	0.00	0.00
Total	100.44	100.06	100.41	99.66	100.68	100.23	100.12	100.85	100.99	100.09	100.46	100.22	100.13	99.96	99.54	100.14	99.58
Si	1.871	1.846	1.916	1.872	1.859	1.911	1.872	1.872	1.823	1.922	1.819	1.846	1.817	1.885	1.880	1.864	1.866
Al^{IV}	0.129	0.154	0.084	0.128	0.141	0.089	0.128	0.128	0.177	0.078	0.181	0.154	0.183	0.115	0.120	0.136	0.134
Al^{VI}	0.102	0.129	0.097	0.108	0.121	0.099	0.134	0.089	0.125	0.070	0.132	0.114	0.093	0.087	0.104	0.127	0.130
Ti	0.023	0.026	0.012	0.021	0.016	0.010	0.018	0.021	0.021	0.019	0.021	0.022	0.030	0.022	0.023	0.019	0.019
Cr	0.006	0.003	0.002	0.006	0.005	0.000	0.006	0.013	0.005	0.002	0.008	0.002	0.005	0.002	0.005	0.007	0.000
Fe^{3+}	0.025	0.028	0.008	0.022	0.031	0.013	0.014	0.036	0.065	0.006	0.061	0.043	0.071	0.024	0.013	0.020	0.018
Fe^{2+}	0.206	0.214	0.181	0.167	0.163	0.203	0.186	0.167	0.155	0.209	0.142	0.164	0.142	0.150	0.186	0.192	0.174
Mn	0.007	0.009	0.005	0.004	0.007	0.005	0.007	0.008	0.006	0.004	0.005	0.006	0.004	0.005	0.005	0.004	0.003
Ni	0.000	0.001					0.002	0.000	0.000	0.006							
Mg	0.749	0.727	0.823	0.773	0.762	0.833	0.751	0.778	0.748	0.789	0.734	0.753	0.753	0.805	0.776	0.745	0.749
Ca	0.834	0.807	0.824	0.846	0.846	0.792	0.821	0.838	0.813	0.853	0.835	0.846	0.852	0.864	0.838	0.831	0.854
Na	0.048	0.057	0.046	0.051	0.048	0.042	0.061	0.051	0.059	0.039	0.062	0.048	0.046	0.041	0.049	0.055	0.053
K	0.000	0.000	0.000	0.000	0.000	0.001	0.000	0.000	0.001	0.000	0.000	0.002	0.000	0.000	0.000	0.000	0.000
Total	4.000	4.001	3.998	3.998	3.999	3.998	4.000	4.001	3.998	3.997	4.000	4.000	3.996	4.000	3.999	4.000	4.000
Wo	46.63	46.17	45.06	47.36	47.77	43.34	46.70	47.01	47.40	46.09	48.81	48.00	48.77	47.50	46.54	47.02	48.07
En	41.88	41.60	45.05	43.28	43.05	45.57	42.74	43.61	43.60	42.62	42.90	42.72	43.12	44.26	43.11	42.13	42.14
Fs	11.50	12.23	9.89	9.36	9.18	11.09	10.57	9.38	9.00	11.29	8.29	9.28	8.11	8.25	10.35	10.86	9.79

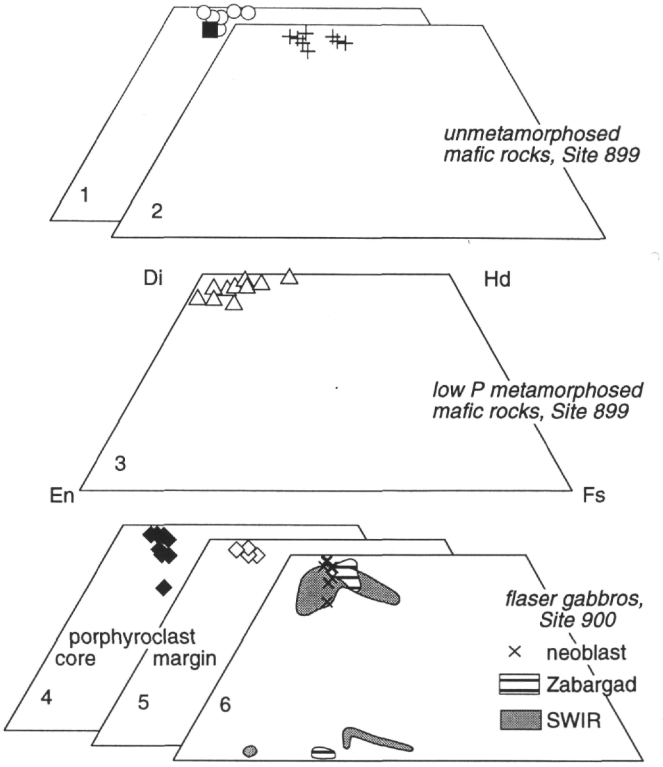

Figure 9. Quadrilateral component diagram for pyroxenes (Di = diopside, Hd = hedenbergite, En = enstatite, Fs = ferrosilite). 1 and 2 are unmetamorphosed mafic rocks from Hole 899B (circle = intragranular lavas, solid square = microgabbros, cross = porphyritic lavas); 3 represents low-pressure and low-temperature metamorphic mafic clasts (open triangle = pyroxene remnants); 4-6 are pyroxene from Site 900 flaser gabbros (filled diamond = porphyroclast core, open diamond = porphyroclast margin, cross = neoblast). The compositional areas of pyroxenes from the Southwest Indian Ridge gabbros (heavy stippling; Hebert et al., 1991) and Zabargad Island gabbros (horizontal hatching; Bonatti and Seyler, 1987; Boudier et al., 1988) are reported for comparison.

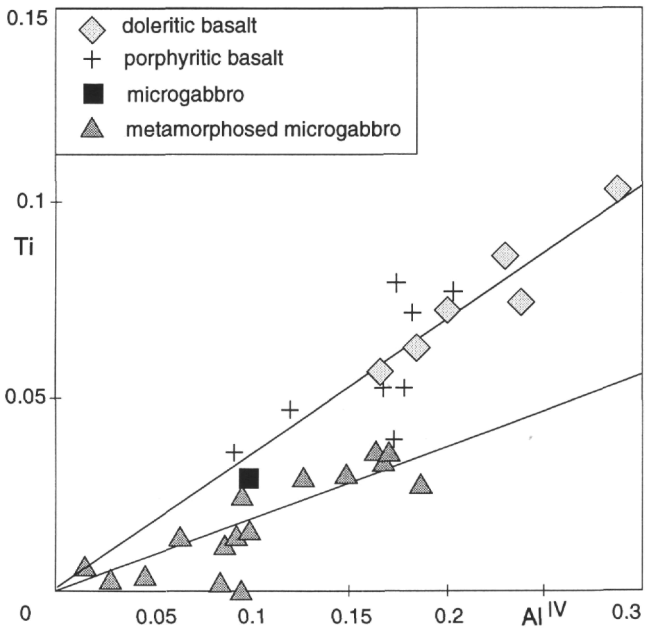

Figure 10. Ti vs. Al^{IV} diagram for clinopyroxenes from mafic clasts recovered at Site 899, Subunit IVA.

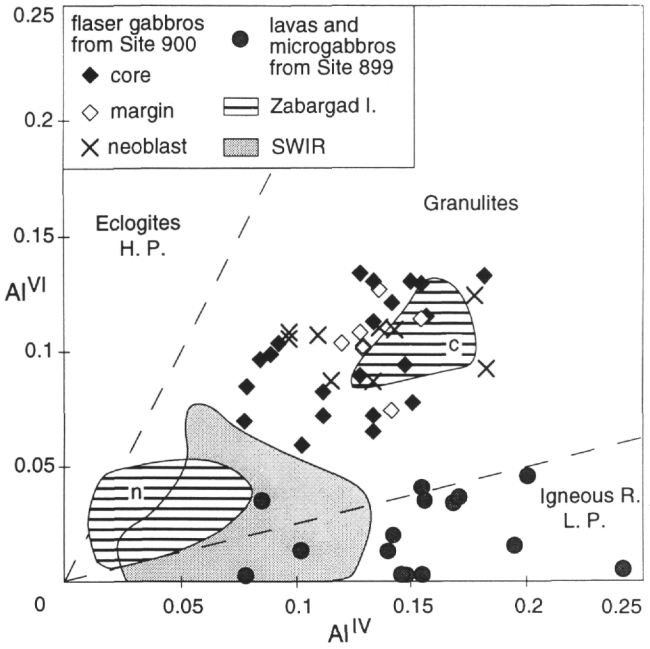

Figure 11. Al^{VI} vs. Al^{IV} diagram for clinopyroxenes from Site 900 flaser gabbros (solid diamonds = porphyroclast core, open diamonds = porphyroclast margin, crosses = neoblast), and from unmetamorphosed lavas and microgabbros from Hole 899B (solid circles). Areas for high, low, and intermediate pressures after Aoki and Shiba (1973), clinopyroxenes from Southwest Indian Ridge (heavy stippling) after Hebert et al. (1991) and Stakes et al. (1991) and from Zabargad Island (horizontal hatching, C = porphyroclast core, N = neoblast) after Bonatti et al. (1987) and Boudier et al. (1988).

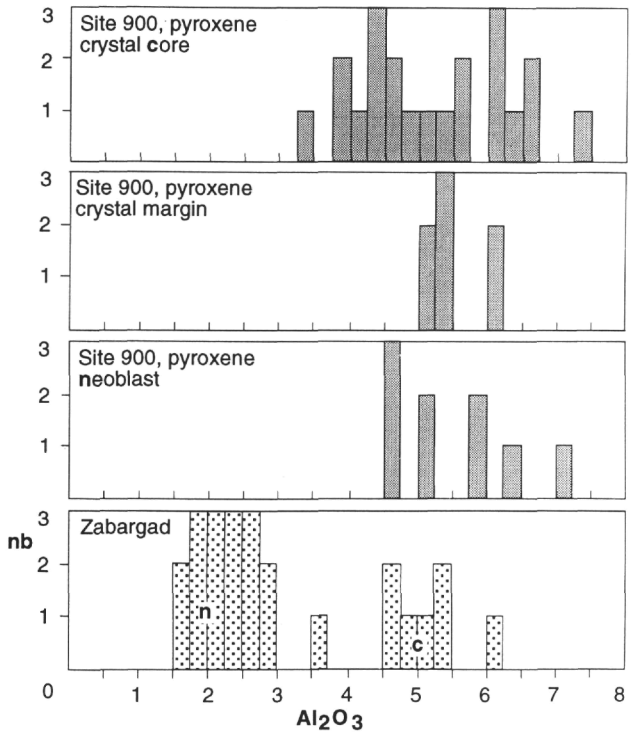

Figure 12. Al_2O_3 content histograms for clinopyroxenes from Site 900 flaser gabbro and from Zabargad metagabbros (data after Bonatti et al., 1987; Boudier et al., 1988); c = porphyroclast core, n = neoblast.

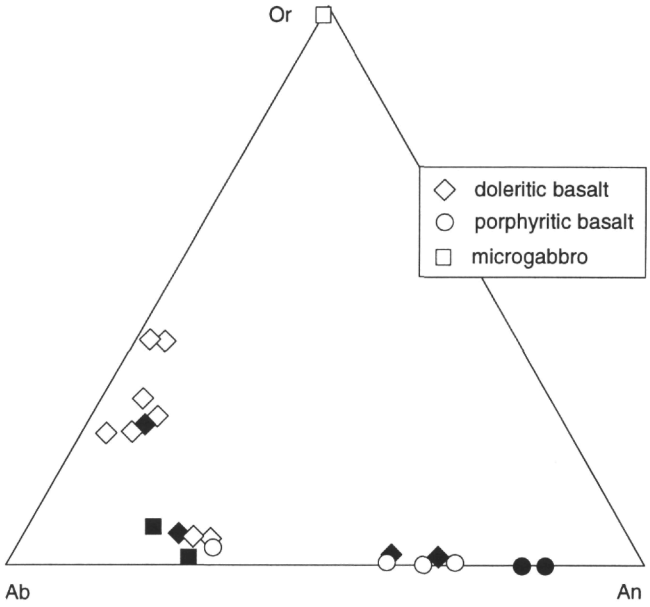

Figure 13. Feldspar composition of unmetamorphosed lavas and microgabbro reported in the triangular main component diagram (Or = orthoclase, Ab = albite, An = anorthite). Solid symbols = phenocrystal core, open symbols = phenocrystal margin and microcrystal.

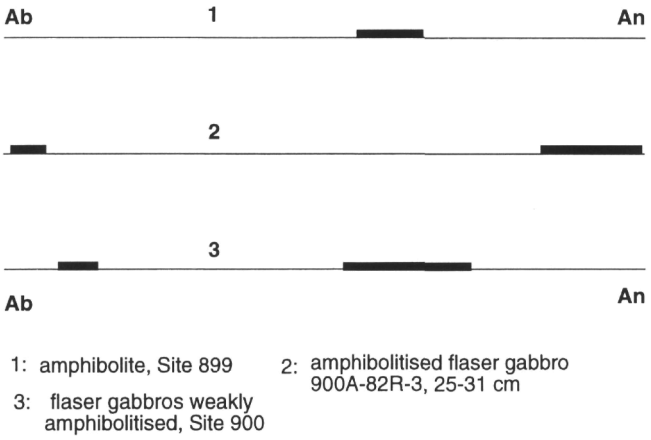

Figure 14. Composition of plagioclase in sheared amphibolite from Hole 899B and in flaser gabbros from Hole 900A. Porphyroclasts and neoblasts have the same composition. Those rich in albite correspond to pervasive albitization areas for both types of crystal.

groups of mafic clasts: those with about 0.6% and others with 1%-2% TiO_2. Their Mg# between 83% and 90% are also comparable and indicative of low differentiation.

The REE-normalized patterns of prehnite-bearing mafic clasts fit those of unmetamorphosed lavas and show tholeiitic and alkaline affinities as well. The absence of a Ce anomaly points to the absence of important LREE mobility, and consequently preserved the reliability and significance of La_N/Ce_N ratios (Gotten et al., 1995).

The composition of the ripidolite clast and chlorite-schist boulder are largely related to that of the chlorite phase, which constitutes more than 90% of the clasts. These rocks show high Al_2O_3 content and a severe depletion in Si and alkali elements. Their chondrite-normalized pattern is flat at about 25 times chondrites, with Ce_N/Yb_N = 1.24 and a marked negative Eu anomaly. They have a relatively high Tb content that correlates with the presence of titanite (Fig. 19). Their REE pattern is identical to those from plagiogranites (Gerlach et al., 1981; Pedersen and Malpas, 1984; Lécuyer et al., 1991). It is also very similar to that of the chlorite-bearing schist (Ga186-10) recovered at the top of the ultramafic section on the Galicia Margin with, however, some differences (Schärer et al., 1995). The latter, indeed, shows larger concentrations of LREE (60 times chondrites rather than 25), is richer in Ni (226 ppm vs. 89 ppm), and poorer in Cr (15 ppm vs. 239 ppm).

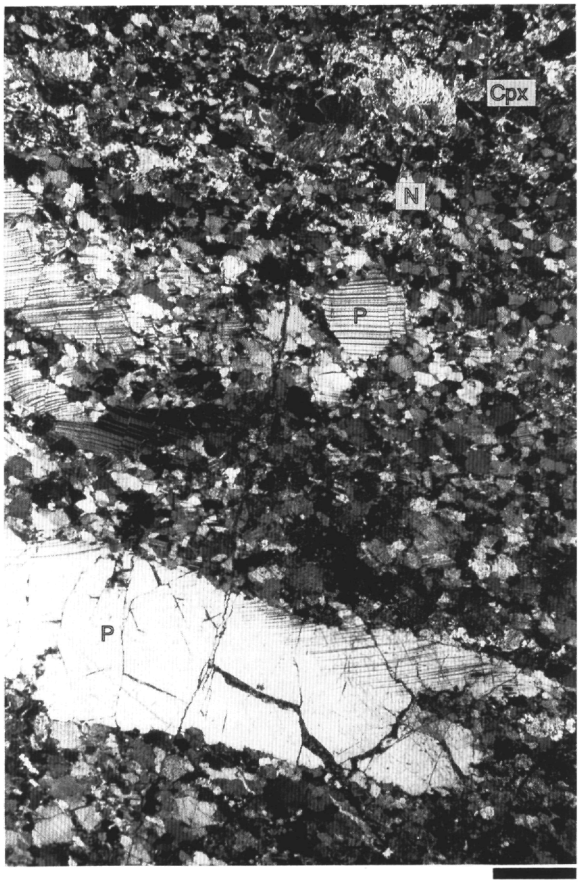

Figure 15. Photomicrograph (using crossed polars) of the coarse-grained flaser gabbro (Sample 149-900A-85R-1, 83-88 cm). Note that the plagioclase porphyroclasts (P) are bent and rimmed by plagioclase neoblasts (N) because of high-temperature ductile deformation. Few pyroxene neoblasts (Cpx) are visible. Scale bar = 1 mm.

The flaser gabbros from Hole 900A have LOI between 2.7 and 9.27 wt%. Up to LOI = 4 wt%, LOI and Rb or Sr contents are positively correlated; above this value, Rb and Sr decrease drastically. The high LOI contents are closely related to the presence of secondary minerals: chlorite, amphibole, and epidote. According to IUGS nomenclature, the fresher rocks would correspond to magmas akin to subalkali basalts. Their Ni content ranges between 90 and 400 ppm, with a relatively high mean centered around 200 ppm. Ni increases slowly with depth and correlates with Mg#, which varies between 80% and 87%. TiO_2 and V variations show a clear gradient: they increase from the top of the basement section down to 758 mbsf (Section 149-900A-81R-1), where they reach the maximum of around 1.1%, then decrease regularly downhole. There is no obvious gradient for Zr.

A fine-grained flaser gabbro (Sample 149-900A-85R-1, 63-67 cm) displays a weak enrichment in REE concentrations, by 2.5 to 6.5 times chondrite (Fig. 19). Its pattern is relatively flat, with an obvious positive Eu anomaly related to the accumulation of plagioclase crystals, and La_N/Ce_N = 0.91 and Ce_N/Yb_N = 0.81. Other typical sections have patterns that do not differ greatly from the Ti-rich ones, which

Table 2. Selected analyses of feldspars.

Hole:	899B					899B					899B					899B			899B				
Core, section:	27R-1					27R-1					28R-2					34R-1			34R-1				
Interval (cm):	27–30					33–40					8–10					37–42			10–15				
Sample:	Porphyritic basalt					Doleritic basalt					Doleritic basalt					Microgabbro			Amphibolite				
Site:	C	M	μ	μ	μ	C	C	M	μ	μ	C	C	M	μ	μ	C	M	μ	C	M	N	N	v
Major elements:																							
SiO_2	46.28	51.71	50.32	52.40	59.66	62.14	64.93	65.60	60.82	65.89	51.73	53.63	66.23	66.70	67.03	60.97	64.42	64.40	53.07	52.15	52.32	53.87	62.67
TiO_2	0.03	0.10	0.04	0.05	0.12	0.00	0.13	0.12	0.04	0.00	0.08	0.07	0.13	0.15	0.08	0.02	0.00	0.00	0.02	0.00	0.04	0.01	0.00
Al_2O_3	34.06	30.46	31.39	29.20	24.84	23.51	20.24	19.40	24.23	19.38	30.33	28.73	20.06	18.58	19.25	24.03	18.14	17.91	29.58	30.23	30.43	29.41	18.80
Fe_2O_3	0.22	0.39	0.35	0.68	0.94	0.43	0.57	0.30	0.24	0.65	0.54	0.67	0.47	0.67	0.60	0.36	0.28	0.19	0.00	0.00	0.07	0.15	0.02
MgO	0.19	0.21	0.23	0.59	0.56	0.03	0.45	0.05	0.03	0.00	0.14	0.41	0.23	0.00	0.00	0.05	0.65	0.03	0.00	0.01	0.01	0.01	0.00
CaO	17.14	13.44	14.47	12.16	6.35	5.06	1.81	0.90	6.22	1.35	13.86	12.24	1.55	0.40	0.81	5.67	0.02	0.00	12.39	13.01	13.01	11.65	0.00
Na_2O	1.78	3.94	3.39	4.54	7.52	8.09	7.27	6.10	7.55	7.29	3.62	4.39	7.57	6.47	8.45	8.02	0.12	0.16	4.75	4.00	4.15	4.99	0.18
K_2O	0.00	0.00	0.04	0.06	0.53	0.98	4.21	6.71	0.83	5.15	0.24	0.37	4.05	6.93	4.12	0.24	15.11	15.67	0.00	0.00	0.00	0.03	15.86
Total	99.70	100.25	100.22	99.68	100.53	100.23	99.60	99.18	99.96	99.71	100.53	100.51	100.28	99.91	100.32	99.35	98.74	98.36	99.81	99.39	100.04	100.13	97.52
Or	0.0	0.0	0.2	0.3	3.1	5.6	25.1	40.1	4.7	29.7	1.4	2.1	24.0	40.5	23.4	1.4	98.7	98.5	0.00	0.00	0.00	0.18	98.30
Ab	15.8	34.7	29.7	40.2	66.1	70.2	65.9	55.4	65.5	63.8	31.6	38.5	68.2	57.5	72.8	70.9	1.2	1.5	40.90	35.75	36.58	43.60	1.70
An	84.2	65.3	70.1	59.5	30.8	24.3	9.0	4.5	29.8	6.5	67.0	59.4	7.8	2.0	3.8	27.7	0.1	0.0	59.10	64.25	63.42	56.22	0.00

Hole:	900A				900A				900A	900A		900A				900A			900A		
Core, section:	80R-2				81R-1				82R-3	84R-4	84R-4			85R-1		85R-4			85R-5		
Interval (cm):	91–94				44–49				25–31	67–72	131–133			21–24		114–120			30–32		
Sample:	Amphibolitized flaser gabbro									Flaser gabbro											
Site:	C	M	N	N	C	M	N	N	N	N	N	N	C	N	C	N	N	C	M	N	
Major elemtents:																					
SiO_2	51.00	50.82	50.77	55.14	55.53	55.55	55.41	46.93	54.06	52.69	65.23	53.54	52.16	52.18	53.28	54.11	50.88	51.54	51.94		
TiO_2	0.04	0.02	0.00	0.00	0.01	0.00	0.02	0.00	0.06	0.04	0.00	0.04	0.00	0.03	0.00	0.00	0.00	0.07	0.02		
Al_2O_3	31.83	31.41	31.80	27.98	28.27	28.38	28.55	33.89	28.53	29.99	21.93	29.61	30.56	30.22	29.96	28.78	30.73	31.12	30.58		
Fe_2O_3	0.00	0.04	0.11	0.02	0.07	0.17	0.00	0.00	0.13	0.13	0.20	0.05	0.04	0.00	0.21	0.13	0.06	0.29	0.09		
MgO	0.01	0.00	0.00	0.01	0.00	0.00	0.00	0.02	0.00	0.00	0.00	0.03	0.02	0.01	0.00	0.00	0.01	0.00	0.00		
CaO	15.03	14.62	15.10	11.50	10.40	10.35	10.78	16.90	11.88	12.55	2.88	12.33	13.67	13.38	12.88	11.92	14.35	13.72	13.61		
Na_2O	3.16	3.45	3.20	5.36	5.87	5.74	5.66	1.59	4.96	4.35	10.08	4.39	3.91	3.96	4.09	4.76	3.43	3.80	3.75		
K_2O	0.08	0.08	0.06	0.11	0.00	0.05	0.00	0.00	0.20	0.16	0.03	0.15	0.18	0.15	0.12	0.19	0.13	0.05	0.15		
Total	101.15	100.44	101.04	100.13	100.14	100.24	100.42	99.41	99.82	99.92	100.35	100.15	100.53	99.93	100.55	99.89	99.59	100.59	100.13		
Or	0.40	0.40	0.30	0.60	0.00	0.30	0.00	0.00	1.10	0.90	0.2	0.9	1.0	0.9	0.7	1.1	0.8	0.3	0.9		
Ab	27.40	29.80	27.60	45.50	50.50	50.00	48.70	14.55	42.60	38.20	86.2	38.9	33.7	34.6	36.2	41.5	30.0	33.3	33.0		
An	72.10	69.80	72.00	53.90	49.50	49.80	51.30	85.45	56.30	60.90	13.6	60.3	65.2	64.5	63.0	57.4	69.3	66.4	66.1		

Notes: C = core of phenocryst or porphyroclast, M = margin, μ = microcryst, N = neoblast. Or, Ab, An = molecular proportion of orthoclase, albite, and anorthite.

Table 3. Selected analyses of magnetites and spinels.

Hole:	899B		899B		899B		900A			
Core, section:	27R-1		28R-2		34R-1		85R-1			
Interval (cm):	33–40		8–10		10–15		21–24			
	Magnetite				Spinel					
Sample:	Doleritic basalts				Amphibolite		Flaser gabbro			
Site:	C	μ	μ	μ	N	N	N	N	N	N
Major elements:										
SiO_2	3.24	0.89	0.10	0.07	0.00	0.02	0.06	0.01	0.00	0.03
TiO_2	18.31	18.92	21.56	21.52	0.00	0.02	0.22	0.22	0.12	0.14
Al_2O_3	3.46	3.28	0.95	1.70	63.00	61.78	54.29	54.12	58.98	60.86
Cr_2O_3	0.00	0.00	0.06	0.00	0.21	0.09	5.11	5.31	1.08	0.84
FeO	63.71	66.14	64.61	64.98	22.91	25.28	29.08	29.53	29.14	24.03
MnO	3.88	4.24	5.07	4.89	0.18	0.38	0.53	0.26	0.55	0.18
MgO	1.74	0.47	0.00	0.00	12.47	11.27	8.04	9.04	9.45	13.33
NiO			0.14	0.13	0.17	0.23				
Total	96.76	96.80	95.13	95.92	99.03	99.25	97.32	98.48	99.32	99.41
Si	0.121	0.034	0.004	0.003	0	0	0.002	0.000	0.000	0.001
Ti	0.515	0.543	0.641	0.632	0	0	0.005	0.005	0.003	0.003
Al	0.153	0.147	0.044	0.078	1.981	1.961	1.828	1.796	1.901	1.910
Cr	0	0	0.002	0	0.005	0.002	0.115	0.118	0.023	0.018
Fe^{3+}	0.575	0.699	0.664	0.652	0.015	0.035	0.044	0.076	0.070	0.065
Fe^{2+}	1.416	1.413	1.471	1.469	0.496	0.535	0.651	0.620	0.596	0.470
Mn	0.123	0.137	0.17	0.162	0.004	0.009	0.013	0.006	0.013	0.004
Mg	0.097	0.027	0	0	0.496	0.453	0.342	0.379	0.385	0.529
Ni			0.004	0.004	0.004	0.005				
Total	3.000	3.000	3.000	3.000	3.000	3.000	3.000	3.000	3.000	3.000
Mg#					49.80	45.44	34.44	37.94	39.25	52.96
Cr#					0.25	0.10	5.92	6.17	1.20	0.93

Notes: C = core of phenocryst, μ = microcryst, N = inclusions in plagioclase neoblasts. Formula unit calculated on the basis of 4 oxygens. Mg# = 100 × Mg/(Mg + Fe + Mn), Cr# = 100 × Cr/(Cr + Al).

Table 4. Selected analyses of ilmenites.

Hole:	899B		899B				899B	899B	900A		900A			
Core, section:	20R-1		27R-1				28R-2	34R-1	81R-1		85R-1			
Interval (cm):	134–136		33–40				8–10	37–42	44–49		83–88			
Sample:	Metamicrogabbro (clast)		Doleritic basalts					Micro-gabbro	Amphibolitized flaser gabbro		Flaser gabbro			
Site:											C	C	M	N
Major elements:														
SiO_2	0.09	0.00	0.12	0.05	0.00	0.01	0.03	0.00	0.00	0.03	0.00	0.02	0.03	0.02
TiO_2	50.83	50.56	47.95	47.54	47.73	48.00	47.11	49.68	50.78	49.99	55.17	55.22	52.63	52.88
Al_2O_3	0.02	0.00	0.31	0.33	0.36	0.32	0.15	0.00	0.04	0.01	0.00	0.04	0.00	0.03
Cr_2O_3	0.03	0.00	0.10	0.00	0.02	0.00	0.00	0.20	0.12	0.23	0.15	0.26	0.21	0.07
FeO	46.12	47.32	46.11	47.61	46.15	47.94	46.76	44.90	46.06	45.79	28.18	36.36	43.23	44.56
MnO	2.12	2.07	0.40	0.59	0.82	0.76	0.88	2.78	2.28	2.28	16.09	6.97	3.37	2.49
MgO	0.26	0.14	2.41	2.41	2.46	2.46	1.03	0.67	0.20	0.22	0.50	0.63	0.63	0.40
CaO	0.02	0.04	0.03	0.01	0.05	0.00	0.02	0.00	0.08	0.16	0.09	0.00	0.00	0.18
Total	99.85	100.68	98.39	99.74	98.65	100.73	96.88	98.76	99.55	98.70	100.18	99.50	100.10	100.62
Si	0.002	0.000	0.003	0.001	0.000	0.000	0.001	0.000	0.000	0.001	0.000	0.001	0.001	0.000
Ti	0.001	0.000	0.911	0.893	0.905	0.893	0.920	0.953	0.965	0.956	1.042	1.051	0.993	0.994
Al	0.966	0.955	0.009	0.010	0.011	0.009	0.005	0.000	0.001	0.000	0.000	0.001	0.000	0.001
Cr	0.001	0.000	0.002	0.000	0.000	0.000	0.000	0.004	0.002	0.005	0.003	0.005	0.004	0.001
Fe^{3+}	0.062	0.089	0.160	0.203	0.179	0.205	0.154	0.090	0.067	0.082	0.000	0.000	0.008	0.009
Fe^{2+}	0.913	0.905	0.814	0.792	0.794	0.786	0.861	0.868	0.906	0.891	0.592	0.769	0.899	0.922
Mn	0.045	0.044	0.009	0.013	0.017	0.016	0.019	0.060	0.049	0.049	0.342	0.149	0.072	0.053
Mg	0.010	0.005	0.091	0.090	0.092	0.091	0.040	0.025	0.007	0.008	0.019	0.024	0.024	0.015
Ca	0.000	0.001	0.001	0.000	0.001	0.000	0.000	0.000	0.002	0.004	0.002	0.000	0.000	0.005
Total	2.000	2.000	2.000	2.000	2.000	2.000	2.000	2.000	2.000	2.000	2.000	2.000	2.000	1.999
Mg#	1.03	0.52	9.96	10.06	10.19	10.19	4.35	2.62	0.73	0.84	1.96	2.51	2.37	1.50

Notes: C = core, M = margin of crystals, N = neoblast. Formula unit calculated on the basis of 3 oxygens. Mg# = 100 × Mg/(Mg + Fe + Mn).

seem a little more depleted in LREEs. Such high and relatively flat patterns are unusual for typical gabbros of mid-ocean ridges (Allégre et al., 1973; Noiret et al., 1981), and for ophiolitic gabbros, as in the Oman complex (Pallister and Knight, 1981; Ernewein et al., 1988), which are more LREE depleted and similar to typical MORB.

DISCUSSION

The unmetamorphosed lavas and microgabbros from Site 899 have a wide range of compositions which overlaps the tholeiitic and transitional fields, some lavas having alkaline affinities (Fig. 18). The porphyritic lavas and microgabbros have flat tholeiitic-like patterns that do not exhibit the common LREE depletion of N-MORBs. These flat patterns, with $La_N/Ce_N > 1$ and $Ce_N/Yb_N > 1$, fit the characteristics of E-MORB well (Sun and McDonough, 1989). Other lavas are clearly transitional in composition.

Such compositional trends are common in lavas from rifted continental margins. Those recovered on the Galicia Margin display quite similar tholeiitic to alkaline trends (Kornprobst et al., 1988). However, they have higher heavy REE (HREE) content (11 times chondrite, at least) and some of them are LREE depleted, like true MORBs. Lavas and dolerites from Zabargad Island (Petrini et al., 1988) also display the same compositional fan as the Galician lavas,

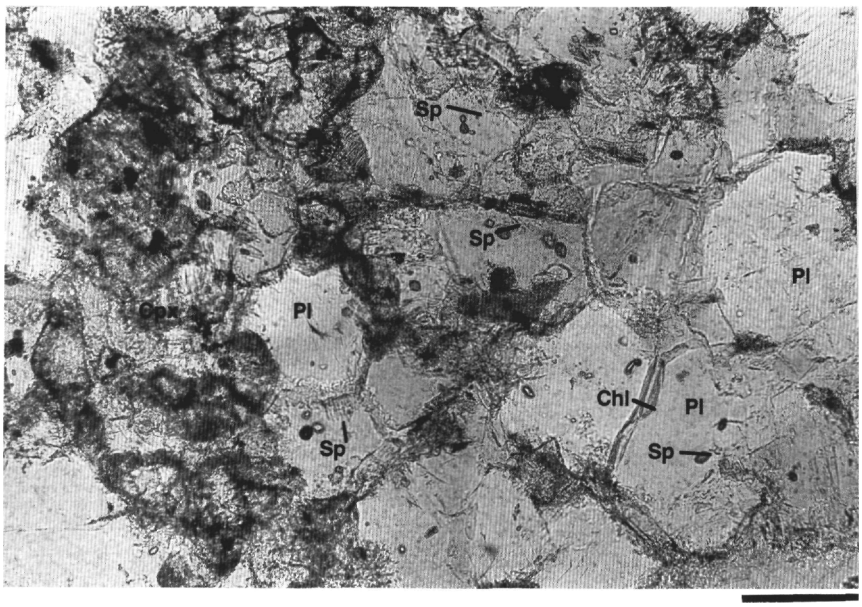

Figure 16. Photomicrograph of green spinel inclusions (Sp) within plagioclase neoblasts (Pl) in a flaser gabbro (Sample 149-900A-80R-2, 127-132 cm). Notice the polygonal shapes of plagioclase neoblasts, their chlorite rims (Chl), and the scarce relics of pyroxene neoblasts (Cpx). Scale bar = 0.2 mm.

Table 5. Selected analyses of amphiboles and biotites from lavas and undeformed gabbros.

Hole:	899B	899B			899B		899B
Core, section:	28R-2	34R-1			28R-2		34R-1
Interval (cm):	8–10	37–42			8–10		37–42
Sample:	Doleritic basalt	Microgabbro			Doleritic basalt		Micro-gabbro
Mineral:		Amphibole			Biotite		
Major elements:							
SiO_2	39.13	50.08	49.83	51.02	36.65	37.19	38.58
TiO_2	4.92	2.71	3.13	2.72	7.11	7.29	5.18
Al_2O_3	10.76	2.20	1.36	1.67	12.50	12.32	11.14
Cr_2O_3	0.00	0.00	0.02	0.00	0.00	0.06	0.12
Fe_2O_3	0.00	0.97	3.27	7.17			
FeO	22.04	17.54	21.07	13.56	19.24	18.26	19.30
MnO	0.43	0.17	0.41	0.41	0.21	0.16	0.12
MgO	5.90	10.57	7.06	10.92	11.52	11.31	13.32
CaO	11.01	6.59	4.88	5.27	0.03	0.02	0.00
Na_2O	2.50	5.00	5.52	5.47	0.78	0.93	0.77
K_2O	1.19	0.78	0.71	0.61	8.17	8.12	8.23
Cl	0.02	0.04	0.06	0.00	0.02	0.01	0.05
H_2O	1.91	1.97	1.94	2.04	3.96	3.96	3.99
Total	99.80	98.61	99.24	100.84	100.23	99.64	100.78
(–O = Cl)	0.00	–0.01	–0.01	0.00	–0.01	0.00	–0.01
Total	99.79	98.60	99.23	100.84	100.22	99.64	100.77
Si	6.113	7.569	7.645	7.505	5.540	5.622	5.783
Al^{IV}	1.887	0.391	0.245	0.289	2.227	2.195	1.968
Al^{VI}	0.093	0.000	0.000	0.000	0.000	0.000	0.000
Ti	0.578	0.308	0.361	0.301	0.808	0.829	0.584
Cr	0.000	0.000	0.003	0.000	0.000	0.003	0.005
Fe^{3+}	0.000	0.105	0.356	0.765			
Fe^{2+}	2.879	2.222	2.724	1.696	2.432	2.309	2.418
Mn	0.057	0.022	0.053	0.051	0.027	0.021	0.015
Mg	1.374	2.382	1.613	2.393	2.594	2.549	2.976
Ca	1.842	1.067	0.801	0.831	0.005	0.003	0.000
Na_B	0.158	0.933	1.199	1.169	0.230	0.272	0.224
Na_A	0.598	0.532	0.444	0.389			
K	0.238	0.150	0.139	0.114	1.575	1.566	1.573
Cl	0.004	0.009	0.016	0.000	0.005	0.003	0.012
OH	1.996	1.991	1.984	2.000	3.995	3.997	3.988
Total	17.816	17.681	17.583	17.503	19.442	19.369	19.545
Mg#	31.88	51.49	36.74	57.80	51.34	52.24	55.02

Note: Formula units calculated on the basis of 23 oxygens and 2 (OH, F, Cl) for amphiboles, 22 oxygens and 4 (OH, F, Cl) for biotites. H_2O is calculated assuming stoichiometry. Mg# = 100 × Mg/(Mg + Fe + Mn)

with the same order of HREE contents but with slightly higher LREE ones in the most enriched samples.

Differences between the Leg 149 lavas and those from Galicia Bank and Zabargad Island are slight. Compared to the latter, the Leg 149 lavas do not display any LREE depletion and are HREE poorer (10 times less), even for the more enriched samples. This would indicate that the sources at the origin of the Iberia Abyssal Plain lavas retained HREE better or were more depleted in HREE. Because of the high content of incompatible elements, we suggest that the magmas from which the Leg 149 lavas originated formed at relatively high pressure through low degrees of partial mantle melting that probably involved garnet-bearing zones.

The prehnite-bearing mafic metamorphic clasts recovered at the same site retain textural (porphyritic or intergranular) and mineralogical (pyroxenes) evidence that points to the origins of the lava. Their geochemical signatures are in fact quite similar to those of the un-

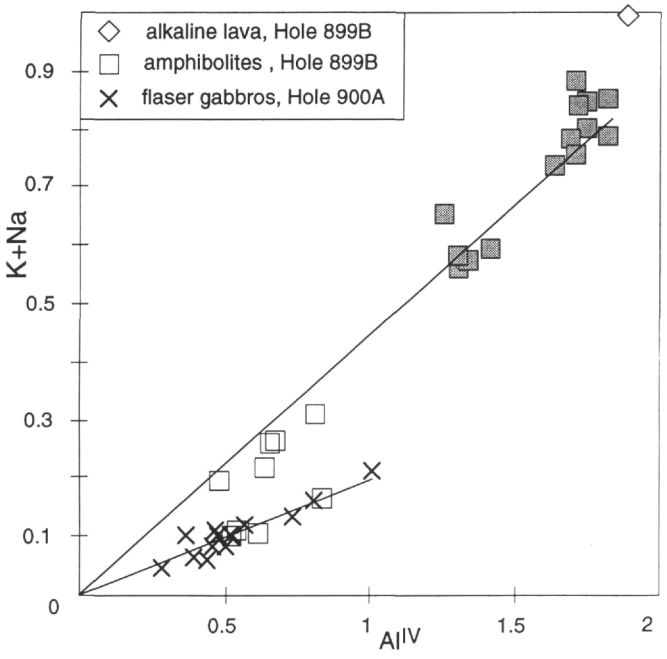

Figure 17. Al^{IV} vs. Na + K diagram for calcic amphiboles from mafic rocks of Sites 899 and 900. Open and cross symbol = low-temperature amphiboles, solid symbol = high-temperature amphiboles (brown).

metamorphosed lavas and microgabbros (Fig. 18). Some have a tholeiitic signature, others have transitional to alkaline affinities. The high Mg# of the pyroxenes in the metamorphic clasts point to a lesser degree of differentiation for these clasts compared to the clasts of unmetamorphosed rocks.

The clasts and boulders dominated by chlorite (ripidolite) are peculiar metamorphic rocks, the origin of which is debatable. Petrological and chemical arguments have shown that such rocks may result from the combined effects of hydrothermal alteration and compressive strain operating on leucogabbros during magma cooling (Essaifi et al., 1995). Those recovered from the Galicia Bank were interpreted as derived from a differentiated and underplated Fe-Ti gabbro, deformed during the late stages of the continental rifting. They provided primitive zircon with a U/Pb age of 122.1 Ma, which is in close agreement with the previous results obtained on this margin (Schärer et al., 1995). Those recovered at Site 899 have flat REE patterns that fit those of leucogabbros or plagiogranite perfectly. Their REE concentrations (20-25 times chondrite), combined with a Ce_N/Yb_N of 1.24 and the absence of La and Ce depletion, would be indicative of undepleted tholeiitic or transitional affinities for these differentiated magmas.

The sheared amphibolite sampled at the bottom of Hole 899B have all the mineralogical and geochemical characteristics of the Site 900 flaser gabbros, apart from the occurrence of Cl-rich titanian pargasites. Although the chronology of amphibole crystallization must be determined, it seems that these former gabbros underwent a high-amphibolite-grade metamorphism, close to granulite facies conditions, which allowed crystallization of green spinels (pleonaste) and titanian pargasites. Later, the primary clinopyroxenes and brown amphiboles were replaced by lower-grade amphiboles.

The flaser gabbros from Site 900 and the sheared amphibolites from Site 899 are obviously different from the undeformed microgabbros, whether prehnite-bearing or not, recovered from Site 899. The former indeed contain high-temperature and high-pressure phases such as green spinel, Na- and Al-rich pyroxenes, or titanian pargasite, which are indicative of metamorphism under high-pressure conditions (about 0.8 GPa). Because the syntectonic recrystallization process leading to the transformation of porphyroclasts into neoblasts is not marked by any Al or Na decrease for pyroxene, and Ca for plagioclase, it is inferred that the high-pressure and high-temperature conditions were still operating during the shearing event.

The major- and trace-element compositions of the flaser gabbros correspond to those of tholeiitic magmas. Their relatively high REE concentrations, their LREE content up to 2.7 times chondrite, and their Ce_N/Yb_N of 0.81 are unusual in MORB-type gabbros, unless it is assumed that they represent a differentiated fraction of "primitive" MORB-like magma (Allègre et al., 1973). The latter point is consistent with the high Mn contents of their Fe-Ti oxides but not with the high Mg# and Ni content of bulk rocks. Their La_N/Ce_N of about 1 are also unusual for MORB-like magmas, even if differentiated, and fit better those of transitional magmas that form at the beginning of rifting (Dupuy and Dostal, 1984; Sun and McDonough, 1989; Arndt et al., 1993). The age close to 136 Ma of the last low-grade metamorphic event that imprinted the gabbros at Site 900 (Féraud et al., this volume) is consistent with an origin related to the last magmatic episodes of the continental rifting (Féraud et al., this volume).

At present, no equivalent of these flaser gabbros is known on the Galicia Bank, or on shore from Iberia. The dredges performed immediately northward have produced very different rocks: quartz-, sericite- and chlorite-bearing schists on the Vasco de Gama Seamount, and orthogneiss and coarse-grained garnet-, orthopyroxene-, and biotite-bearing granulites on Vigo Seamount (Capdevila and Mougenot, 1988). These granulites, the origins of which are dubious, have Archean ages (Guerrot et al., 1990; Capdevila, pers. comm., 1994).

CONCLUSIONS

Our mineralogical and chemical data provide new information about the nature, metamorphic evolution, and origin of the mafic rocks recovered during Leg 149 in the Iberia Abyssal Plain.

The low-grade metamorphosed or unmetamorphosed lavas and microgabbros present in the cataclastic breccia at Site 899 derived from the crystallization of E-MORB to alkaline-type magmas. These rocks possibly crystallized from magmas that originated from different sources or from a homogeneous melt, later contaminated by an enriched subcontinental mantle. Some of the mafic rocks, and particularly the chlorite-bearing schists, may be considered to be former differentiated Fe-Ti leucogabbros or plagiogranites, which were later hydrothermally modified under low-temperature and -pressure conditions. The associated sheared amphibolites are the hydrated equivalent of the flaser gabbros recovered eastward at Site 900.

The flaser gabbros have no equivalent on shore. Their composition is slightly different from typical mid-ocean ridge gabbros and fits better the compositions of transitional magmas and their differentiated products, which form at the beginning of rifting (Dupuy and Dostal 1984; Sun and McDonough 1989; Arndt et al., 1993). These former gabbros subsequently underwent an intense shearing under relatively high-temperature (high amphibolite to granulite facies) and high-pressure ($\geq$0.8 Gpa) conditions, which is not compatible with crystallization under a mature oceanic ridge. This shearing ended under lower-grade metamorphic conditions around 136 Ma (Féraud et al., this volume).

The flaser gabbros would therefore have crystallized from transitional to tholeiitic-type magmas ponded and slowly cooled at the base of continental crust, and subsequently sheared during continental stretching. As thinning proceeded, the decrease of pressure combined with an increase of the permeability and of the amount of pervasive hydrothermal fluids allowed dynamic metamorphism under granulite to amphibolite facies conditions followed subsequently by static greenschist facies conditions. The oldest lavas, presumed to pour out during this stage, at present bear only a low-pressure prehnite-chlorite imprint.

ACKNOWLEDGMENTS

We are indebted to M. Bohn, E. Boeuf, A. Cossard, and R. Derval for their technical skill, to J. Gotten (Brest University), M. Polve (Toulouse University), and C. Monnier (Nantes University) for geochemical analyses. We also thank C. Mével and M. Cannai for their careful reviews. This work was supported by CNRS grants (Geoscience Marine).

REFERENCES

Agrinier, P., Mével, C., and Girardeau, J., 1988. Hydrothermal alteration of the peridotites cored at the ocean/continent boundary of the Iberian Margin: petrologic and stable isotope evidence. *In* Boillot, G., Winterer, E.L., et al., *Proc. ODP, Sci. Results,* 103: College Station, TX (Ocean Drilling Program), 225-234.

Allègre, CJ., Montigny, R.,and Bottinga, Y., 1973. Cortège ophiolitique et cortège océanique, géochimie comparée et mode de genèse. *Bull. Soc. Geol. Fr.,* 7:461-477.

Aoki, K., and Shiba, I., 1973. Pyroxenes from lherzolite inclusions of Itinome-gata, Japan. *Lithos,* 6:41-51.

Arndt, N.T., Czamanske, O.K., Wooden, J.L., and Fedorenko, V.A., 1993. Mantle and crustal contributions to continental flood volcanism. *Tectonophysics,* 223:39-52.

Beslier, M.-O., Ask, M., and Boillot, G., 1993. Ocean-continent boundary in the Iberia Abyssal Plain from multichannel seismic data. *Tectonophysics,* 218:383-393.

Beslier, M.-O., Girardeau, J., and Boillot, G., 1990. Kinematics of peridotite emplacement during North Atlantic continental rifting, Galicia, NW Spain. *Tectonophysics,* 184:321-343.

Bloomer, S.H., Natland, J.H., and Fisher, R.L., 1989. Mineral relationships in gabbroic rocks from fracture zones of Indian Ocean ridges: evidence for extensive fractionation, parental diversity, and boundary-layer recrystallization. *In* Saunders, A.D., and Norry, MJ. (Eds.), *Magmatism in the Oceanic Basins.* Geol. Soc. Spec. Publ. London, 42:107-124.

Boillot, G., Comas, M.C., Girardeau, J., Kornprobst, J., Loreau, J.-P., Malod, J., Mougenot, D., and Moullade, M., 1988a. Preliminary results of the Galinaute cruise: dives of the submersible *Nautile* on the Western Galicia Margin, Spain. *In* Boillot, G., Winterer, E.L., et al., *Proc. ODP, Sci. Results,* 103: College Station, TX (Ocean Drilling Program), 37-51.

Boillot, G., Girardeau, J., and Kornprobst, J., 1988b. Rifting of the Galicia Margin: crustal thinning and emplacement of mantle rocks on the seafloor. *In* Boillot, G., Winterer, E.L., et al., *Proc. ODP, Sci. Results,* 103: College Station, TX (Ocean Drilling Program), 741-756.

Boillot, G., Grimaud, S., Mauffret, A., Mougenot, D., Kornprobst, J., Mergoil-Daniel, J., and Torrent, G., 1980. Ocean-continent boundary off the Iberian margin: a serpentinite diapir west of the Galicia Bank. *Earth Planet. Sci. Lett.,* 48:23-34.

Boillot, G., Winterer, E.L., et al., 1988. *Proc. ODP, Sci. Results,* 103: College Station, TX (Ocean Drilling Program).

Bonatti, E., and Seyler, M., 1987. Crustal underplating and evolution in the Red Sea rift: uplifted gabbro/gneiss crustal complexes on Zabargad and Brothers islands. *J. Geophys. Res.,* 92:12803-12821.

Boudier, F., Nicolas, A., Ji, S., Kienast, J.R., and Mével, C., 1988. The gneiss of Zabargad Island: deep crust of a rift. *Tectonophysics,* 150:209-227.

Capdevila, R., and Mougenot, D., 1988. Pre-Mesozoic basement of the western Iberian continental margin and its place in the Variscan Belt. *In* Boillot, G., Winterer, E.L., et al., *Proc. ODP, Sci. Results,* 103: College Station, TX (Ocean Drilling Program), 3-12.

Cotten, J., Le Dez, A., Bau, M., Caroff, M., Maury, R.C., Dulski, P., Fourcade, S., Bohn, M., and Brousse, R., 1995. Origin of anomalous rare-earth element and yttrium enrichments in subaerially exposed basalts: evidence from French Polynesia. *Chem. Geol.,* 119:115-138.

Dupuy, C., and Dostal, J., 1984. Trace element geochemistry of some continental tholeiites. *Earth Planet. Sci. Lett.* 67:61-69.

Ernewein, M., Pflumio, C., and Whitechurch, H., 1988. The death of an accretion zone as evidenced by the magmatic history of the Sumail Ophiolite (Oman). *Tectonophysics,* 151:247-274.

Essaifi, A., Capdevila, R., and Lagarde, J.L., 1995. Transformation de leucogabbros en chloritoschistes sous l'effet de l'altération hydrothermale et de la déformation dans l'intrusion de Kettara (Jebilet, Maroc). *C. R. Acad. Sci. Ser. 2,* 320:189-196.

Féraud, G., Girardeau, J., Beslier, M.O., and Boillot, G., 1988. Datation $^{39}Ar/^{40}Ar$ de la mise en place des péridotites bordant la marge de la Galice (Espagne). *C. R. Acad. Sci. Ser. 2,* 307:49-55.

Frost, B.R., 1976. Limits to the assemblage forsterite-anorthite as inferred from peridotite hornfelses, Icicle Creek, Washington. *Am. Mineral.,* 61:732-750.

-------- , 1991. Stability of oxide minerals in metamorphic rocks. *In* Lindsley, D.H. (Ed.), *Oxide Minerals: Petrologic and Magnetic Significance.* Mineral. Soc. Am., Rev. Mineral., 25:469-487.

Frost, B.R., and Lindsley, D.H., 1991. Occurrence of iron-titanium oxides in igneous rocks. *In* Lindsley, D.H. (Ed.), *Oxide Minerals: Petrologic and Magnetic Significance.* Mineral. Soc. Am., Rev. Mineral., 25:433-468.

Gamble, R.P., and Taylor, L.A., 1980. Crystal/liquid partitioning in augite: effects of cooling rate. *Earth Planet. Sci. Lett.,* 47:21-33.

Gerlach, D.C., Avé Lallemant, H.G., and Leeman, W.P., 1981. An island arc origin for the Canyon Mountain Ophiolite complex, Eastern Oregon, U.S.A. *Earth Planet. Sci. Lett.,* 53:255-265.

Guérin, H., Brousse, R., and Maury, R.C., 1979. Comportement du manganèse au cours de la cristallisation fractionnée de séries alcalines. *Chem. Geol.,* 24:83-95.

Guerrot, C., Peucat, J.J., Capdevila, R., and Dosso, L., 1990. Reply to the comment of Kuijper, R.P., *on* "Archan protoliths within Early Proterozoic granulitic crust of the West European Hercynian belt: possible relics of the Western craton." Geology, 18:382-383

Hébert, R., Constantin, M., and Robinson, P.T., 1991. Primary mineralogy of Leg 118 gabbroic rocks and their place in the spectrum of oceanic mafic igneous rocks. *In* Von Herzen, R.P., Robinson, P.T., et al., *Proc. ODP, Sci. Results,* 118: College Station, TX (Ocean Drilling Program), 3-20.

Helmstaedt, H., and Allen, J.M., 1977. Metagabbronorite from DSDP Hole 334: an example of high temperature deformation and recrystallization near the Mid-Atlantic ridge. *Can. J. Earth Sci.,* 14:886-898.

Honnorez, J., Mével, C., and Montigny, R., 1984. Geotectonic significance of gneissic amphibolites from the Verna fracture zone, equatorial Mid-Atlantic Ridge. *J. Geophys. Res.,* 89:11379-11400.

Ito, E., and Anderson, A.T., Jr., 1983. Submarine metamorphism of gabbros from the Mid-Cayman Rise: petrographic and mineralogie constraints on hydrothermal processes at slow-spreading ridges. *Contrib. Mineral. Petrol.,* 82:371-388.

Kornprobst, J., Vidal, P., and Malod, J., 1988. Les basaltes de la marge de Galice (NO de la Péninsule Ibérique): hétérogénéité des spectres de terres rares à la transition continent/océan. Données géochimiques préliminaires. *C.R. Acad. Sci. Ser. 2,* 306:1359-1364.

Larsen, L.M., 1976. Clinopyroxenes and coexisting mafic minerals from the alkaline Ilimaussaq intrusion, South Greenland. *J. Petrol,* 17:258-290.

Leake, B.E., 1978. Nomenclature of amphiboles. *Can. Mineral,* 16:501-520.

Lécuyer, C., Brouxel, M., and Lapierre, H., 1991. Petrogenesis of magmas at a fossil slow-spreading center: the Trinity ophiolite (northern California, USA). *Bull. Soc. Geol Fr.,* 162:795-809.

Liou, J.G., Maruyama, S., and Cho, M., 1985. Phase equilibria and mineral parageneses of metabasites in low-grade metamorphism. *Mineral Mag.,* 49:321-333.

Noiret, G., Montigny, R., and Allègre, C., 1981. Is the Vourinos Complex an island arc ophiolite? *Earth Planet. Sci. Lett.,* 56:375-386.

Pallister, J.S., and Knight, RJ., 1981. Rare-earth element geochemistry of the Samail ophiolite near Ibra, Oman. *J. Geophys. Res.,* 86:2673-2697.

Pedersen, R.B., and Malpas, J., 1984. The origin of oceanic plagiogranites from the Karmoy Ophiolite, western Norway. *Contrib. Mineral. Petrol.,* 88:36-52.

Petrini, R., Joron, J.L., Ottonello, G., Bonatti, E., and Seyler, M., 1988. Basaltic dykes from Zabargad island, Red Sea: petrology and geochemistry. *Tectonophysics,* 150:229-248.

Schärer, U., Kornprobst, J., Beslier, M.O., Boillot, G., and Girardeau, J., 1995. Gabbro and related rock emplacement beneath rifting continental crust: U-Pb geochronological and geochemical constraints for the Galicia passive margin (Spain). *Earth Planet. Sci. Lett.,* 130:187-200.

Shipboard Scientific Party, 1994a. Site 897. *In* Sawyer, D.S., Whitmarsh, R.B., Klaus, A., et al., *Proc. ODP, Init. Repts.,* 149: College Station, TX (Ocean Drilling Program), 41-113.

-------- , 1994b. Site 899. *In* Sawyer, D.S., Whitmarsh, R.B., Klaus, A., et al., *Proc. ODP, Init. Repts.,* 149: College Station, TX (Ocean Drilling Program), 147-209.

-------- , 1994c. Site 900. *In* Sawyer, D.S., Whitmarsh, R.B., Klaus, A., et al., *Proc. ODP, Init. Repts.,* 149: College Station, TX (Ocean Drilling Program), 211-262.

Stakes, D., Mével, C., Cannat, M., and Chaput, T., 1991. Metamorphic stratigraphy of Hole 735B. *In* Von Herzen, R.P., Robinson, P.T., et al., *Proc. ODP, Sci. Results,* 118: College Station, TX (Ocean Drilling Program), 153-180.

Sun, S.-S., and McDonough, W.F., 1989. Chemical and isotopic systematics of oceanic basalts: implications for mantle composition and processes. *In* Saunders, A.D., and Norry, MJ. (Eds.), *Magmatism in the Ocean Basins.* Geol. Soc. Spec. Publ. London, 42:313-345.

Von Herzen, R.P., Robinson P.T., Natland, J.H., Meyer, P.S., Dick, J.B., and Bloomer, S.H., 1991. Magmatic oxides and sulfides in gabbroic rocks from Hole 735B and the later development of the liquid line of descent. *In* Von Herzen, R., Robinson, P.T., et al., *Proc. ODP, Sci. Results,* 118: College Station, TX (Ocean Drilling Program), 75-111.

Whitmarsh, R.B., Miles, P.R., and Mauffret, A., 1990. The ocean-continent boundary off the western continental margin of Iberia, I. Crustal structure at 40°30'N. *Geophys. J. Int.,* 103:509-531.

Whitmarsh, R.B., Pinheiro, L.M., Miles, P.R., Recq, M., and Sibuet, J.C., 1993. Thin crust at the western Iberia ocean-continent transition and ophiolites. *Tectonics,* 12:1230-1239.

Whitney, P.R., 1972. Spinel inclusions in plagioclase of metagabbros from Adirondack Highlands. *Am. Mineral.,* 57:1429-1436.

Date of initial receipt: 2 January 1995
Date of acceptance: 17 July 1995 Ms
149SR-220

Table 6. Selected analyses of amphiboles from amphibolites and flaser gabbros.

Hole:	899B						900A			900A			900A					900A	900A
Core, section:	34R-1						81R-1			82R-5			84R-4		85R-1			85R-4	85R-6
Interval (cm):	10–15						44–49			25–29			131–133		21–24			114–120	140–145
Sample:	Amphibolite						Amphibolitized flaser gabbro						Flaser gabbro						
Major elements:																			
SiO_2	41.79	42.77	42.65	51.22	53.60	49.50	51.84	51.32	52.30	50.06	52.58	52.70	53.20	55.16	53.23	53.13	54.20	54.00	51.00
TiO_2	2.49	2.82	2.77	0.29	0.22	0.13	0.35	0.75	0.09	0.36	0.13	0.20	0.05	0.14	0.04	0.05	0.16	0.18	0.77
Al_2O_3	13.22	12.05	12.43	5.23	2.93	7.45	4.02	4.49	3.06	5.95	4.19	4.01	3.77	2.50	3.83	4.35	3.51	3.11	5.53
Cr_2O_3	0.15	0.35	0.30	0.10	0.00	0.00	0.03	0.00	0.04	0.26	0.08	0.25	1.29	0.00	0.02	0.04	0.01	0.00	0.23
Fe_2O_3	1.79	0.96	2.19	7.47	5.67	2.66	8.32	7.05	2.85	3.36	2.70	0.77	1.60	1.19	2.66	5.61	1.80	5.55	4.56
FeO	10.72	11.40	9.15	3.66	5.49	6.38	4.13	7.61	11.77	9.76	11.42	11.50	8.61	7.65	7.91	6.23	8.09	5.41	4.19
MnO	0.23	0.02	0.27	0.14	0.29	0.11	0.27	0.22	0.24	0.16	0.37	0.29	0.29	0.16	0.07	0.17	0.19	0.25	0.11
MgO	11.87	12.62	13.15	17.57	17.69	16.59	16.73	15.23	14.50	14.24	14.53	15.26	16.32	18.30	17.11	16.77	17.13	17.46	17.95
CaO	11.81	12.13	11.58	11.98	12.16	12.15	11.78	12.14	12.73	12.40	12.81	13.06	12.76	13.19	12.97	12.32	12.70	12.31	12.84
Na_2O	2.41	2.38	2.72	1.08	0.70	1.66	0.30	0.41	0.20	0.45	0.30	0.38	0.29	0.18	0.36	0.44	0.35	0.21	0.57
K_2O	0.31	0.40	0.39	0.08	0.01	0.08	0.12	0.05	0.05	0.04	0.00	0.01	0.01	0.00	0.00	0.01	0.03	0.02	0.03
Cl	0.85	1.24	0.91	0.25	0.13	0.26	0.12	0.24	0.01	0.01	0.00	0.00	0.01	0.00	0.00	0.00	0.00	0.00	0.01
F	0.00					0.02													
H_2O	1.80	1.72	1.82	2.07	2.10	2.01	2.08	2.05	2.07	2.06	2.10	2.10	2.11	2.14	2.12	2.14	2.13	2.14	2.12
Total	99.44	100.85	100.32	101.13	100.99	99.00	100.10	101.56	99.91	99.10	101.20	100.53	100.31	100.60	100.33	101.24	100.36	100.79	100.14
(–O = Cl)	–0.19	–0.28	–0.20	–0.06	–0.03	–0.06	–0.03	–0.06	0.00	0.00	0.00	0.00	0.00	0.00	0.00	0.00	0.00	0.00	0.00
(–O = F)	0.00					–0.01													
Total	99.25	100.57	100.11	101.07	100.96	98.94	100.07	101.50	99.91	99.10	101.20	100.53	100.31	100.60	100.33	101.24	100.36	100.79	100.14
Si	6.204	6.286	6.247	7.187	7.518	7.107	7.346	7.273	7.570	7.263	7.493	7.533	7.544	7.718	7.523	7.435	7.632	7.560	7.189
Al^{IV}	1.796	1.714	1.753	0.813	0.482	0.893	0.654	0.727	0.430	0.737	0.507	0.467	0.456	0.282	0.477	0.565	0.368	0.440	0.811
Al^{VI}	0.518	0.374	0.394	0.051	0.003	0.368	0.017	0.022	0.091	0.281	0.196	0.207	0.174	0.130	0.161	0.152	0.215	0.073	0.107
Ti	0.278	0.312	0.305	0.030	0.023	0.014	0.038	0.080	0.010	0.039	0.014	0.021	0.005	0.015	0.005	0.006	0.016	0.018	0.082
Cr	0.017	0.040	0.035	0.011	0.000	0.000	0.003	0.000	0.005	0.029	0.009	0.028	0.145	0.000	0.003	0.004	0.001	0.000	0.026
Fe^{3+}	0.194	0.103	0.236	0.781	0.590	0.283	0.878	0.737	0.301	0.358	0.281	0.081	0.167	0.123	0.277	0.582	0.187	0.576	0.479
Fe^{2+}	1.337	1.405	1.127	0.436	0.652	0.771	0.499	0.917	1.434	1.194	1.370	1.377	1.025	0.898	0.941	0.738	0.957	0.641	0.499
Mn	0.029	0.002	0.033	0.017	0.035	0.014	0.032	0.027	0.030	0.020	0.044	0.035	0.034	0.018	0.008	0.020	0.023	0.030	0.012
Mg	2.627	2.764	2.870	3.674	3.698	3.550	3.534	3.217	3.129	3.079	3.087	3.251	3.449	3.817	3.605	3.498	3.595	3.644	3.771
Ca	1.879	1.910	1.817	1.801	1.826	1.869	1.789	1.843	1.974	1.928	1.956	2.001	1.938	1.977	1.964	1.847	1.915	1.846	1.939
Na_B	0.121	0.090	0.183	0.199	0.174	0.131	0.081	0.113	0.026	0.072	0.044	0.000	0.062	0.023	0.036	0.120	0.085	0.057	0.061
Na_A	0.573	0.587	0.589	0.094	0.016	0.329	0.000	0.000	0.031	0.055	0.038	0.106	0.018	0.024	0.063	0.000	0.011	0.000	0.094
K	0.058	0.075	0.072	0.015	0.001	0.015	0.022	0.008	0.008	0.008	0.000	0.002	0.002	0.000	0.000	0.001	0.006	0.003	0.005
Cl	0.215	0.309	0.225	0.058	0.031	0.062	0.030	0.058	0.002	0.002	0.000	0.000	0.002	0.000	0.000	0.000	0.000	0.000	0.002
F	0.000					0.009													
OH	1.785	1.691	1.775	1.942	1.969	1.929	1.970	1.942	1.998	1.998	2.000	2.000	1.998	2.000	2.000	2.000	2.000	2.000	1.998
Total	17.631	17.662	17.661	17.109	17.018	17.345	16.892	16.965	17.039	17.063	17.038	17.108	17.020	17.024	17.063	16.968	17.017	16.907	17.099
Mg#	66.27	66.30	71.80	89.39	85.01	82.16	86.94	77.31	68.13	72.06	69.26	70.25	77.09	80.95	79.30	82.58	78.98	85.04	88.31

Notes: Formula unit calculated on the basis of 23 oxygens and 2 (OH, F, Cl). Mg# = 100 × Mg/(Mg + Fe + Mn). H_2O is calculated assuming stoichiometry.

Table 7. Selected analyses of chlorites.

Hole:	899B	899B		900A	900A
Core, section:	34R-1	37R-1		81R-1	83R-2
Interval (cm):	10–15	28–33		44–49	77–82
Sample:	Amphibolite	Chlorite schist		Amphibolitized flaser gabbro	Flaser gabbro
Major elements:					
SiO_2	30.89	25.21	25.00	27.23	27.69
TiO_2	0.01	0.06	0.00	0.00	0.01
Al_2O_3	17.37	20.73	21.03	20.63	21.20
FeO	16.13	29.44	29.70	19.19	18.81
MnO	0.01	0.23	0.18	0.26	0.12
MgO	23.37	12.56	12.16	20.92	20.07
CaO	0.03	0.04	0.00	0.02	0.03
Na_2O	0.03	0.00	0.00	0.02	0.00
K_2O	0.01	0.00	0.00	0.00	0.00
H_2O	12.06	11.19	11.15	11.85	11.87
Total	99.92	99.46	99.22	100.10	99.80
Si	6.139	5.399	5.373	5.509	5.593
Al^{IV}	1.861	2.601	2.627	2.491	2.407
Al^{VI}	2.206	2.631	2.699	2.428	2.638
Ti	0.001	0.010	0.000	0.000	0.001
Fe^{2+}	2.681	5.273	5.338	3.246	3.177
Mn	0.002	0.042	0.032	0.044	0.020
Mg	6.923	4.010	3.894	6.307	6.040
Ca	0.007	0.009	0.000	0.003	0.006
Na	0.013	0.001	0.000	0.007	0.000
K	0.002	0.000	0.000	0.000	0.001
Total	19.815	19.975	19.964	20.036	9.700
Mg#	72.07	43.00	42.03	65.72	65.39

Note: Formula unit calculated on the basis of 28 oxygens and 16(OH). H_2O is calculated assuming stoichiometry. Mg# = 100 × Mg/(Mg + Fe + Mn).

Table 8. Bulk-rock analyses by ICP-AES and ICP-MS.

Hole:	899B	899B	899B	899B	899B	899B	899B	899B	900A	900A	900A		
Core, section:	20R-1	25R-2	27R-1	27R-1	28R-1	34R-1	35R-1	37R-1	81R-1	82R-3	85R-1		
Interval (cm):	134–136	33–37	15–18	27–30	42–45	10–15	29–33	28–33	44–49	25–31	2–7		
No.:	1	2	3	4	5	6	7	8	9	10	11		
Sample:	Metamicrogabbro	Metabasalt (porphyritic)	Variolitic basalt*	Porphyritic basalt	Metamicrogabbro (porphyritic)	Amphibolite	Microgabbro*	Chlorite schist*	Amphibolitized flaser gabbro	Amphibolitized flaser gabbro	Flaser gabbro*	D.L. (ICP-MS)*	ICP-AES
Major elements (wt%)													
SiO_2	38.50	35.70	46.00	47.10	34.40	41.20	43.60	24.80	49.70	49.20	46.50		
TiO_2	1.29	0.60	1.34	0.69	0.93	0.30	0.85	1.56	0.95	0.41	0.30		
Al_2O_3	17.90	19.34	15.60	20.60	19.39	17.10	18.50	21.65	15.48	18.40	14.90		
Fe_2O_3	8.30	7.65	6.95	6.20	6.70	8.96	7.55	28.00	8.85	5.96	7.41		
MnO	0.14	0.14	0.15	0.16	0.13	0.12	0.12	0.20	0.13	0.09	0.12		
MgO	11.65	13.20	11.65	7.54	16.50	16.05	9.92	9.25	9.28	7.76	11.60		
CaO	15.00	12.90	6.25	10.25	10.10	4.70	3.80	5.05	7.65	10.65	13.65		
Na_2O	0.18	0.12	2.40	2.80	0.13	1.41	1.95	0.01	3.02	2.80	1.52		
K2O	0.02	0.01	1.79	0.22	0.01	1.44	2.50	0.00	0.71	0.77	0.15		
P_2O_5	0.16	0.08	0.25	0.09	0.12	0.05	0.10	0.37	0.04	0.04	0.03		
LOI	7.08	10.16	7.20	4.37	11.01	8.00	10.67	8.90	3.68	4.68	4.18		
Total	100.22	99.90	99.58	100.02	99.42	99.33	99.56	99.85	99.49	100.76	100.26		
Trace and rare-earth elements (ppm)													
Sc	35	25	26	25	27	32	32	41	45	48	46		0.5
V	205	106	183	119	160	115	150	237	223	165	171		3
Cr	195	188	220	202	228	360	250	263	164	367	865		3
Co	33	35	38	37	29	56	65	116	49	36	51		3
Ni	54	145	217	162	80	190	180	105	122	91	225		3
Rb	0.5	0.2	31.9	3.5	0.2	12.2	21.9	0.1	6.0	7.4	1.5		0.5
Sr	38.0	43.0	249.5	225.0	52.0	137.0	127.3	11.1	220.0	336.0	197.3	0.032	1
Y	22.5	15.4	18.9	15.0	16.0	6.8	19.0	34.2	10.5	7.8	5.6	0.004	0.5
Zr	88	33	116	46	57	13	55	158	5	16	7		2
Nb	7.1	2.1	25.7	3.2	5.5	0.4	3.2	12.7	0.5	0.7	0.1	0.025	1
Ba	2.0	3.0	321.5	44.0	1.0	552.0	259.5	1.8	99.0	77.0	24.6	0.022	3
La	6.4	2.2	13.6	3.0	4.7	1.0	3.8	6.0	0.7	1.1	0.6	0.004	1
Ce	17.0	6.0	30.8	7.6	12.0	2.5	9.7	15.0	2.2	2.2	1.6	0.012	2
Nd	12.0	3.9	16.6	5.2	9.0	2.0	7.0	10.1	1.5	1.4	1.8	0.009	2
Sm			3.6				2.0	3.8			0.7	0.004	
Eu	1.1	0.6	1.3	0.7	0.6	0.5	1.1	0.5	0.5	0.5	0.4	0.002	0.2
Gd			3.8				2.7	5.0			0.9	0.004	
Tb			0.6				0.5	1.1			0.2	0.002	
Dy	4.1	2.6	3.5	2.6	3.0	1.1	3.4	7.2	1.9	1.4	1.1	0.003	0.4
Er	2.2	1.5	2.0	1.5	1.6	0.6	2.2	4.2	1.0	0.8	0.6	0.003	1
Yb	2.2	1.7	1.7	1.5	1.6	0.6	2.1	3.3	1.0	0.8	0.6	0.002	0.2
Lu			0.3				0.3	0.5			0.1	0.001	
Mg#	85	87	87	83	91	88	84	57	81	84	86		

Notes: ICP-AES analyses were conducted by J. Cotten at the University of Brest, France. ICP-MS analyses were conducted by C. Monnier and M. Polvé, University of Toulouse, France. Analyses obtained from ICP-AES were calibrated using AC-E, BE-N, KB-2, and MICA-Fe standards, except Rb (atomic absorption). Relative standard deviations were ~2% for major elements and <5% for trace elements. * = trace elements obtained from ICP-MS were calibrated using Dolerite WS-E, Microgabbro PM-S, and BE-N standards. D.L. = detection limits (ppm).

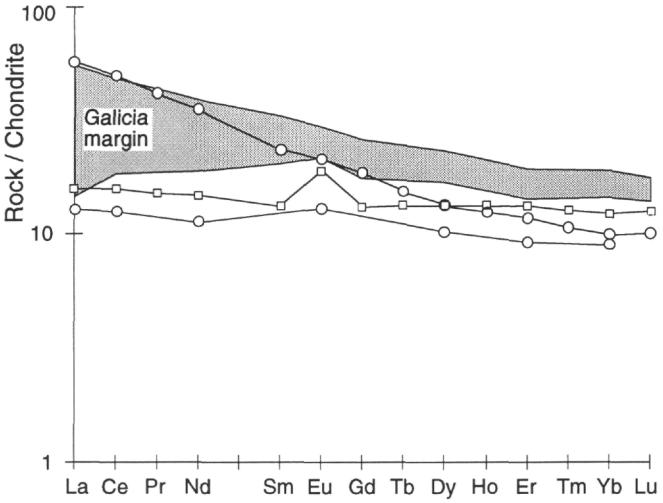

Figure 18. Chondrite-normalized rare-earth-elements pattern for the unmetamorphosed lavas (circles) and microgabbro (squares) from Site 899. The shaded area is that of basalts collected during the Galinaute cruise on the Galicia Margin (Kornprobst et al., 1988). Normalization values are from Sun and McDonough (1989). Analyses were performed by C. Monnier using inductively coupled plasma-mass spectrometry at the Laboratoire de Géochimie, Toulouse, and by J. Cotten using inductively coupled plasma-atomic emission spectroscopy at the University of Brest.

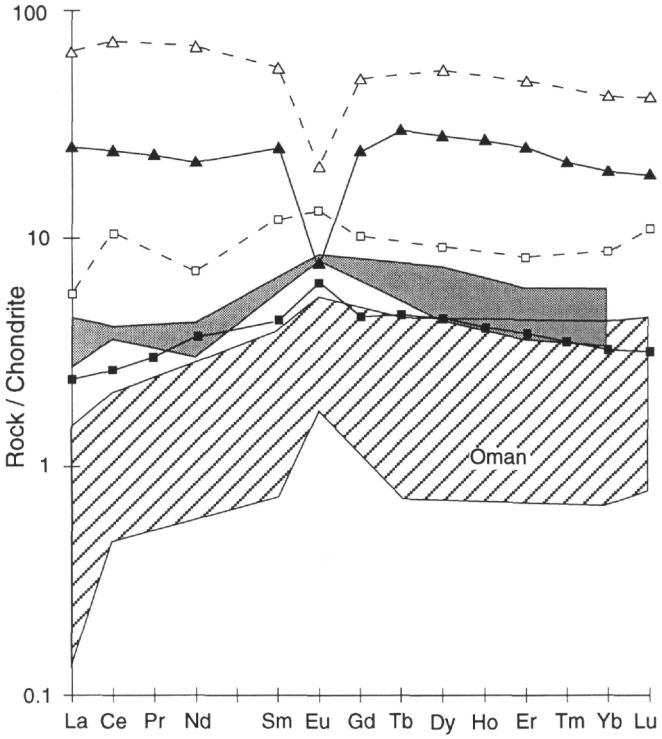

Figure 19. Chondrite-normalized rare-earth-element patterns for the flaser gabbros and related amphibolites. The dark-shaded area represents highly amphibolitized flaser gabbro from Sites 899 and 900. Solid squares represent a pyroxene-rich flaser gabbro from Site 900. The solid triangles represent the chlorite-bearing schist from Site 899. For comparison, this diagram also shows the Oman gabbros with MORB affinities (hatched area) and the gabbro (open square) and chlorite-bearing schist (open triangle) recovered on the Galicia Margin (Schärer et al., 1995).